On stratified jets and wakes generated by a self-propelled body

A Thesis

Submitted for the Degree of

Master of Science (Engineering)

by

Rajapandiyan Asaithambi

Engineering Mechanics Unit
Jawaharlal Nehru Centre for Advanced Scientific Research
(A Deemed University)
Bangalore – 560 064

JUNE 2008

To my family

DECLARATION

I hereby declare that the matter embodied in the thesis entitled "**On stratified jets and wakes generated by a self-propelled body**" is the result of investigations carried out by me at the Engineering Mechanics Unit, Jawaharlal Nehru Centre for Advanced Scientific Research, Bangalore, India under the supervision of Prof. K. R. Sreenivas and that it has not been submitted elsewhere for the award of any degree or diploma.

In keeping with the general practice in reporting scientific observations, due acknowledgment has been made whenever the work described is based on the findings of other investigators.

Rajapandiyan Asaithambi

CERTIFICATE

I hereby certify that the matter embodied in this thesis entitled "**On stratified jets and wakes generated by a self-propelled body**" has been carried out by Mr. Rajapandiyan Asaithambi at the Engineering Mechanics Unit, Jawaharlal Nehru Centre for Advanced Scientific Research, Bangalore, India under my supervision and that it has not been submitted elsewhere for the award of any degree or diploma.

Prof. K. R. Sreenivas
(Research Supervisor)

Acknowledgements

I am indebted to my advisor Prof. K. R. Sreenivas for his constant support and encouragement throughout the time I spent carrying out the work presented in this thesis. Prof. R. Narasimha has been an inspirational figure to me, a person I would try to emulate. Dr. Rao Tatavarthy was very enthusiastic about this project and discussions with him helped me better understand the focus of this thesis. My due thanks to Prof. R. Govindarajan, Prof. J. H. Arakeri, Dr. D. Sengupta, Prof. J. Srinivasan and Dr. O. N. Ramesh for being fantastic teachers and making my classes an enjoyable experience. Mr. Arokianathan, Mr. Srinath and Mr. Srinivas have been ever helpful when I ran into them for tasks big and small I had to get done for the experiments.

I'm grateful to DS and Shivaji for constantly spurring me during these years. I haven't spent better time at JNC than without Harish and Ratul. Thanks to Mukund for being a wonderful colleague and for being all too eager to break the silence in the lab. My hearty thanks to Vinod for patiently teaching me Linux and TT. It was a pleasure to work with Shankar and Sowmitra during the summers. I would like to thank all my friends at the Centre: Aditya, Anubhab, Anjana, Ashish, Bishak, Debu, Gayathri, Gomathi, Kalyani, Kaushik, Kirti, Lakshmi, Mallappa, Mani, Neena, Pinaki, Ponnulakshmi, Priyanka, Punit, Rajaram, Reji, Raji, Sameen, Shreyas, Sikata, Vijay, Vinitha, Vivek, Vivekanand for the memorable two years.

I cannot convey my gratitude in words to Amma, Appa and Naveen for helping me get this far.

Abstract

Wakes in a stratified medium have been studied with considerable interest owing to the ubiquity of such phenomena in nature and engineering applications. In this thesis we have investigated some of the characteristics of wakes/jets generated by propulsive underwater bodies with laboratory-scale experiments using various flow visualization techniques. The qualitative data obtained leads us to some interesting observations and questions. The structure of jets in a stratified flow, to which attention has not been paid in comparison to stratified wakes, has been more closely studied and we have attempted to explain its structure.

We have also used a two-dimensional viscous incompressible flow simulation using the discrete vortex method to construct and test a novel self-propelled body. This model has the potential to yield some insights into the two-dimensional wake decay of a self-propelled body.

List of Figures

Contents

CHAPTER 1

INTRODUCTION

The interest in fluid flow under the influence of density stratification comes naturally as our Earth's atmosphere and oceans are in fact prime examples of such a medium, albiet the length scales at which the stratification is felt is very large. The processes in these media play a very crucial role in determining the climate of the planet and this attracts a wide variety of researchers attempting to understand the behaviour of such flows. However, large man-made objects often feel the effects of stratification and the focus of this thesis lies on the effect of stratification on the wakes and jets produced by such an object, a fully submerged self-propelled vessel.

Turbulent shear flow in a stratified medium is primarily characterized by the inhibition of vertical motion. A discussion of such flows from earlier works is presented in the following pages. The chapter ends with the motivation, objectives and the organisation of this thesis.

1.1 Wakes in stratified fluids

Lin & Pao (1979) describe some of the typical features observed in stratified fluids. The first is the blocking phenomenon often observed upstream of large mountain range and strong turbulence and rotors generated on the downstream side. The same blocking effect results in an upstream wake for a flow across a two-dimensional body. The stratification also inhibits the onset of the vortex street by a cylinder

and can generate internal waves. They discuss the fast decay of vertical velocity as against the other two components observed in a grid-generated turbulence in a stratified fluid. For a turbulent wake generated by a cylinder vertical growth of the wake was limited by the stratification and the entire wake was found to be oscillating at a frequency corresponding to the Brunt-Väisälä frequency. The other phenomenon associated with a turbulent wake was the wake collapse. The mixing in the turbulent wake does work against the density gradient and then collapses vertically to seek its equilibrium position. The process also generates internal waves during the collapse. The far wake after the collapse spreads fast in the lateral direction also forming horizontal vortices. The horizontal vortices are often referred to as pancakes.

Lin *et al.* (1992) performed more elaborate experiments of the flow of a linearly stratified fluid past a sphere with the Froude number ranging from 0.005 to 20 and Reynolds numbers from 5 to $10,000$. They describe eight different flow phenomenon associated with different Froude number, Fr, and Reynolds number, Re, regimes. The flow patterns are very different from those observed in homogeneous fluids. Some of the regimes are briefly descibed here: Low Fr and Re produces steady two dimensional attached vortices. Increasing Re results in an unsteady attached vortices then leading to vortex shedding. The flow is still two-dimensional. Inceasing Fr causes loss in the two-dimensionality with lee waves forming first and becoming unstable. Turbulent wake results at high Fr and Re with a wake spreading out laterally and reaching a maximum height and collapsing vertically.

Schooley & Stewart (1963) studied the wake of self-propelled body. In homogeneous fluid, fluid behind body expands into an irregular conical shape but with stratification, initial expansion is accompanied by spreading in horizontal direction. The fluid behind body has more or less constant density due to mixing. The collaps-

ing vertical wake generates internal waves of high order which manifest in surface movements. They observe that the assumption that internal waves are damped only by viscosity and not by turbulence leads to results in general agreement with their observations.

Bonneton *et al.* (1993) study the internal gravity wave field generated by sphere towed in a stratified fluid with Fr ranging from 1.5 to 12.7 and Re between 380 and $30,000$. They discuss the lee waves and random waves (internal gravity waves) left behind by the sphere and demonstrate that the lee waves are well predicted by linear theory and the random waves are related to coherent structures in the wake.

Chomaz *et al.* (1993*a*) observes the far wake of a sphere towed horizontally in a stratified fluid with $0.25 \leqslant Fr \leqslant 12.7$ and $150 \leqslant Re \leqslant 30,000$. Regardless of Fr the wake becomes quasi two dimensional with respect to the Brunt-Väisälä period. For $Fr \leqslant 4.5$ horizontal motions are coherent over whole depth of wake but above 4.5 it is not and motions are in several layers. This transition occurs smoothly. They importantly observe that horizontal velocity and vertical vorticity diffuse vertically faster than the viscous diffusion law allows and their ratio depends on Re by a mechanism similar to Ekman pumping.

Chomaz *et al.* (1993*b*) identify 4 regimes for the near wake structure of spheres moving in a stratified fluid. For $Fr \geqslant 4.5$, the near wake is similar to a homogeneous case. A triple-layer flow is formed for $Fr \leqslant 0.8$. Close to $Fr = 1$, there is a saturated lee wave and between $1.5 \leqslant Fr \leqslant 4.5$ the wake progressively recovers its behaviour in homogeneous fluid: the axisymmetry of the recirculating zone, the Kelvin-Helmholtz instability and the spiral instability.

1.2 Effect of wake momentum

More recent studies by Voropayev *et al.* (1999) find large vortex structures behind maneouvering (accelerating or taking a turn) bodies in stratified fluids with very slow decay rates. They observe that since $Re \propto t^{-1/3}$ and $Fr \propto t^{-2/3}$ with time the motion becomes horizontal and it is the integral momentum that is now important. This is confirmed by Voropayev & Smirnov (2003) when they observe vortex streets generated by a moving momentum source in stratified fluid. The wake form two momentum sources merge to produce shedding similar to one source. The behaviour of moving jets is also similar to the highly organized vortex streets formed by bluff body wakes indicating that it is only the momentum integral across the wake that matters.

Meunier & Spedding (2004) later describe what they call a memory loss in stratified momentum wakes. They study wakes from objects of different shape but with similar total drag and conclude that the shape does not matter and the wake remembers only the momentum flux given by bluff body and not geometry. This work reinforces the views established by Voropayev & Smirnov (2003).

Meunier & Spedding (2006) have performed experimental study of a propelled bluff body towed a constant speed in stratified fluid. They observe three flow regimes: one depending on thrust/drag ratio, the second is a momentumless regime when the thrust cancels out the drag. A third regime was noticed when the body has a small angle of attack which results in a asymmetric wake. They also argue that a momemtumless regime is a very rare and peculiar flow, rare because a self-propelled body in a stratified fluid will experience viscous and internal wave drag and the wake which essentially contains the viscous wake and jet will have a net positive momentum. The extra momentum generated in the jet to compensate the

wave drag thus remains giving the wake of such a body a positive momentum wake. The experiments were conducted for a Fr between 6 and 40, Re between 5000 and 33000.

1.3 Analytical and numerical studies

Many authors have presented analytical and numerical work in stratified flows. Meunier (2006) present a general model for drag wakes in stratified fluid assuming the wake is self-similar and expands in horizontal direction due to turbulent diffusion and in the vertical direction due to viscous diffusion. The mean characteristics of wake show good agreement with existing numerical and experimental data.

Billant & Chomaz (2001) using self-similarity in strongly stratified inviscid flows propose a scaling law for vertical lengthscales ina stratified fluid. When Fr is small the vertical length scale is self-similar with respect to zN/U, where z is the vertical coordinate. They show that even if the magnitude of vertical velocity is small and scales like FrU, the flow is not two-dimensional.

Fritts *et al.* (2003) numerically simulate a stratified late wake in three dimensions showing excitement of internal waves in the outer flow. They also show that wake velocities are much smaller (as they decay more) for self-propelled bodies than towed bodies over time.

Afanasyev (2004) presents an asymptotic theory for wakes behind towed and self-propelled bodies (in the form of force and force doublets). In Afanasyev & Korabel (2004) an asymptotic theory for starting dipoles is presented. In two dimensional flow a vortex dipole which generates a mushroom like structure similar to those observed by Voropayev *et al.* (1999).

1.4 Surface signatures

There is a lot of interest in studying the surface signatures produced by underwater bodies.

Sheres & Munk (1992) present the data obtained from an earlier researcher. A proposal was made to study wakes of a surface vessle and a snorkeling submarine. The boat had twin screws at $5.7ft$ depth and the submarine also had twin screws at a depth of $46.5ft$. A garden hose placed across the wake drifted with a surface velocity of $\sim 0.3ft/s$ at the centre of the wake immediately after passage of the vessels as shown in Fig. 1.1. The contrasting difference was that the hose which formed a bulge opposite to ship's motion as expected however bulged along the submarine's motion.

Wren & May (1997) discuss many ways of detecting submarines: direct observation, kelvin wake, bernoulli hump, turbulent wake, internal waves affecting the surface, optical effects on surface (such as scattering of light due to wake) and thermal effects of the vessel's heat.

Reed & Milgram (2002) show distinct features of a ship wake from synthetic aperture radar (SAR) imagery. They describe a dark centerline with a bright V flanking the centerline of a typical ship wake. Transverse waves are also occasionally detected.

Melsheimer (2001) also use SAR to identify a ship's dark turbulent wake and often bright but sometimes dark Kelvin wake.

Voropayev *et al.* (2007) analyze detectable signatures on surface caused by submerged momentum disturbances. A momentum source, either a jet or a self-propelled body, was located in the upper homogeneous layer of stable two-layer stratified fluid with a deep lower layer. They define a parameter to describe the

strength of the surface signal in terms of the intensity of the momentum source, the time duration for which it acts and the depth of the upper layer.

1.5 Motivation and Objectives

This study was largely influenced by the need for tracking marine vessels which is of commercial and military importance. Detecting wakes and surface waves of these moving vessels remotely can simplify the process of effectively identifying vessels in vast oceans. This requires us to have a good understanding of the structure of wakes and waves generated by vessels in such an environment. Knowing the effect of wakes and internal waves on the surface helps us in interpreting surface signatures better.

In this thesis, we aim to more closely observe the characteristics of the wake generated by a propelled body in a stratified fluid. Attention is paid to the propelled jet configuration which is not often reported in literature. In an attempt to simulate and study the late wake of a self-propelled body, we employ discrete vortex methods to create and test a simplified model of a self-propelled body.

1.6 Thesis organisation

The experimental setup and a discussion of the observations is presented in the second chapter. The numerical simulation of a model self-propelled body is presented in the third chapter and the fourth chapter is devoted to conclusions.

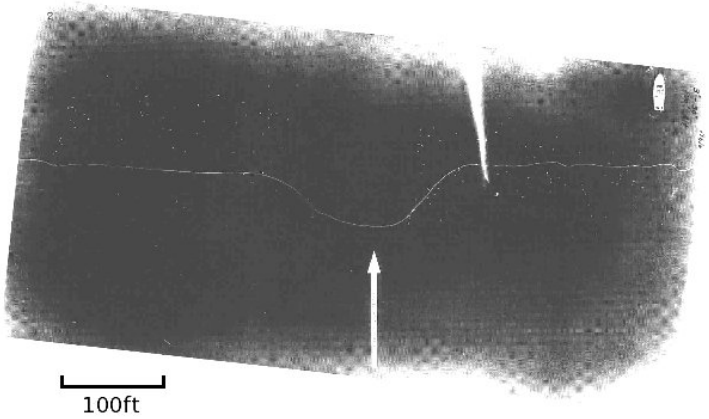

(a) Surface ship

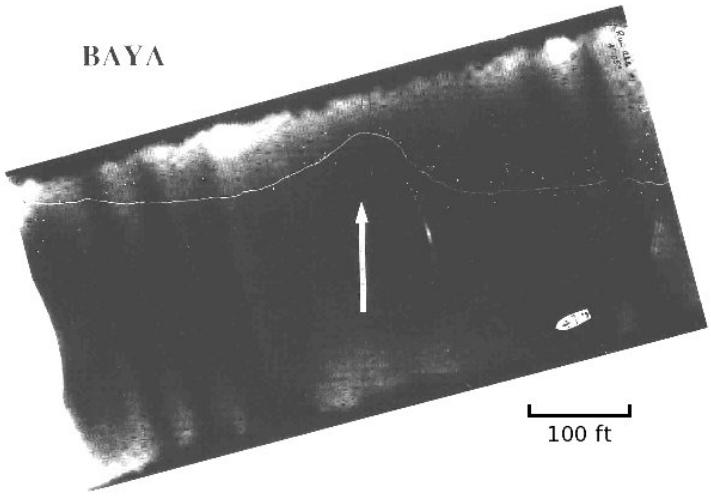

(b) Submarine

Figure 1.1: Aerial pictures of a hose deformed by the wake due to a surface vessel and a submarine

CHAPTER 2

EXPERIMENTAL STUDY

This chapter focuses on the description of the experimental setup, flow visualization techniques employed and the presentation of data collected from the experiments conducted.

2.1 Experimental Setup

2.1.1 Tow tank

The experiments were conducted in a $3000\,mm \times 750\,mm \times 750\,mm$ glass tank. The model to be towed is held firmly from the top with a streamlined sting made of stainless steel (to prevent corrosion). The carriage to which sting is attached can move along the beam that spans the entire length of the tank. The carriage is belt-driven by a computer controlled high-torque microstepping motor capable of $2,000$ steps per revolution. Fig. 2.1 shows the glass tank and the different parts of the towing mechanism. A schematic of the tank with the model being towed in shown in Fig. 2.2

The stepper motor gives us the flexibility of towing the body with an arbitrary velocity as a function of time and is useful for studying straight-line manouevres of a propulsive body. The drawback however that was faced from using the stepper motor is the limited straight-line speeds that could be achieved. Speeds above

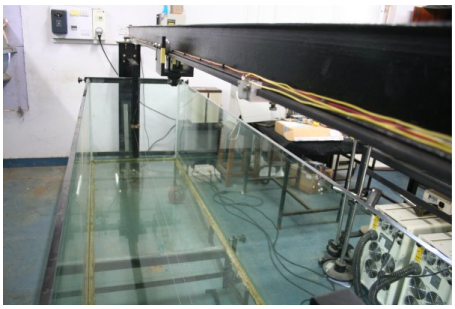

(a) Glass tank and tow rail

(b) Carriage

(c) Motor and belt

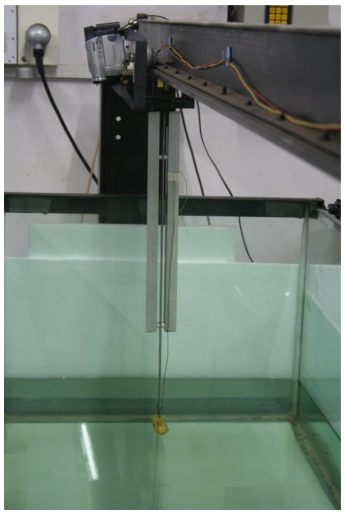

(d) Sting supporting the model

Figure 2.1: Experimental setup

$5cm/s$ caused a lot of vibrations and hence the towing speed for all the experiments conducted were within $2cm/s$.

The towing arrangement and the glass tank are two independent entities and are physically isolated. This prevents any mechanical vibrations due to the motor from being transmitted to the tank.

2.1.2 Stratification

A fluid with varying density is achieved by dissolving varying amounts of salt in water. The two-tank method is commonly used to establish a linear density

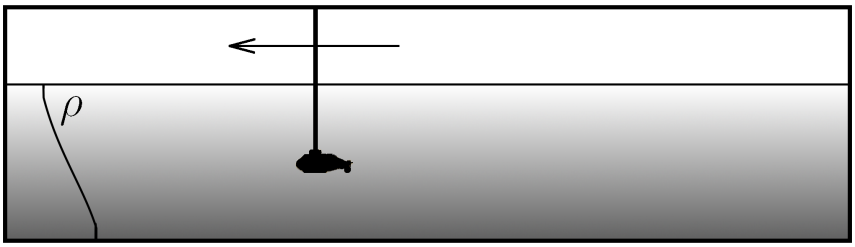

Figure 2.2: A schematic of the tank with the model

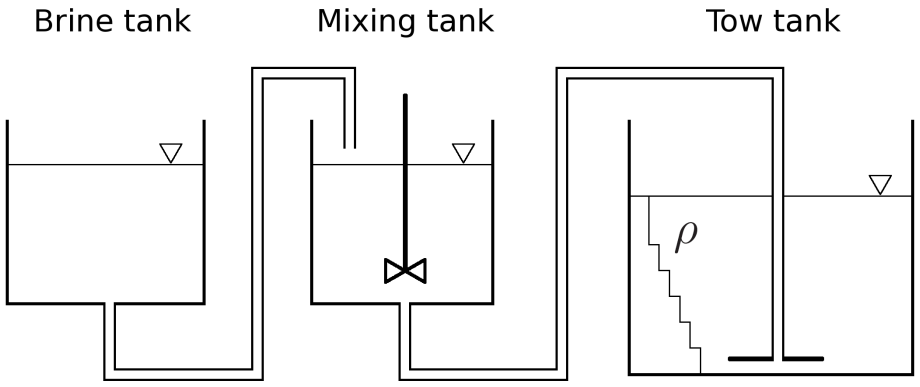

Figure 2.3: Schematic of the two-tank method

stratification. A schematic of this method is shown in Fig. 2.3. Here two tanks, the first filled with brine and the second with fresh water, are the supply tanks. Brine is drained into the mixing tank and the fluid from the mixing tank is in turn drained into the main tank to be used for the experiments. A mixer in the mixing tank ensures that the fluid in it is homogeneous. The salinity is gradually increased as more and more brine is pumped into the mixing tank. The fluid of increasing density from the mixing tank is introduced from the bottom of the main tank. This ensures that no unwanted mixing takes place between fluid layers as the heavier fluid from the mixing tank keeps replaces the lighter fluid in the main tank. The method is accurate in producing a required density profile. The fluid however should not be pumped too fast so as to prevent turbulent mixing with the

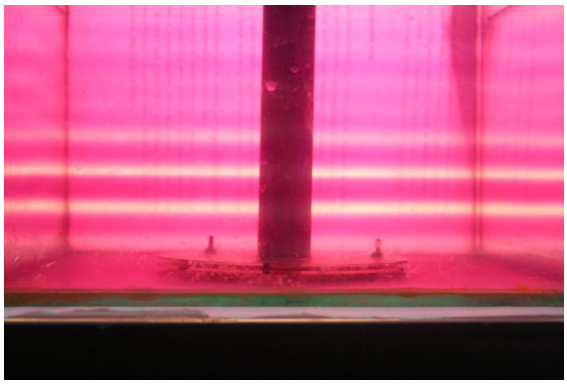

Figure 2.4: Density stratification visualized by alternate coloured layers

lighter upper layers. A circular diffuser along at the bottom of the tank ensures the heavier fluid does not impinge onto the upper layers. There is still the possibility of the shear layer instability occuring between the fast moving heavy fluid and the stagnant lighter fluid and thus the flow rate has to be controlled accordingly. It has been demonstrated by Hill (2002) that any statically stable density profile can be achieved using the two-tank method with computer controlled valves to control the flow rates between the tanks.

However, given the limited resources in this laboratory, the method had to be redesigned and adapted. In our setup, we use only one extra tank. This smaller tank is initially filled with fresh water and a small layer is pumped to the tow tank. Now salt is manually added and mixed to achieve the next density level. The process is discrete and does not produce a continuous stratification like the two-tank method. We end up with finite layers of increasing density. The thickness of each density layer in our filling process was fixed at $10\,mm$. Fig. 2.4 shows the dye-visualization of the density layers created in a smaller tank. The layers are now allowed to diffuse out in time to finally attain a smooth stratification. The one-dimensional diffusion equation is solved to estimate the time we need to wait for the density profile to smoothen out into a linear density stratification. Fig 2.5

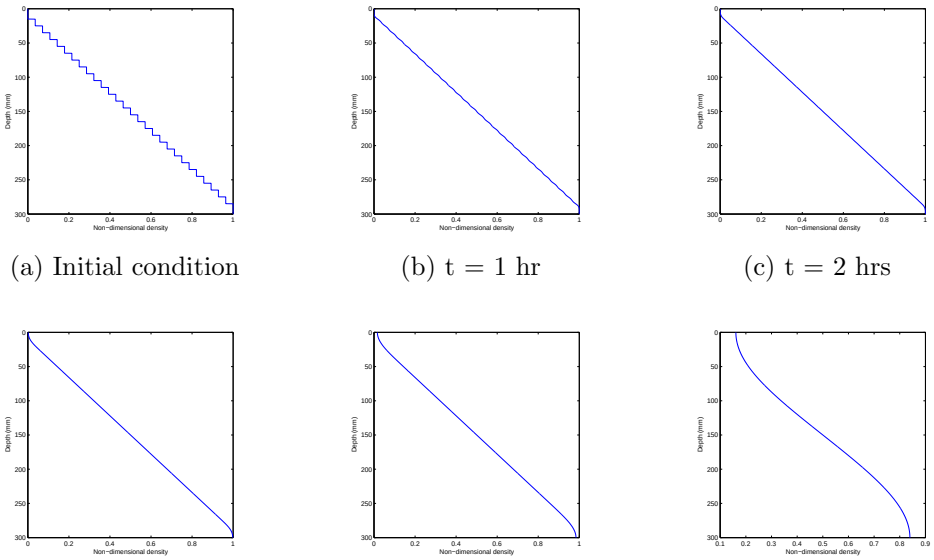

(a) Initial condition (b) t = 1 hr (c) t = 2 hrs

(d) t = 6 hrs (e) t = 1 day (f) t = 20 days

Figure 2.5: Diffusion of salt with time

is a density profile evolving with time as calculated numerically.

The tank is filled to a height of 300 mm for all the experiments. This number follows from the height chosen by Meunier & Spedding (2006) in their work, 260 mm, who found no dependence on this height in experiments performed with a bluff bodies of diameter $\approx 30\,mm$ which is similar to the body we use. The strength of the stratification is characterized by the Brunt-Väisälä frequency, N, defined in Eqn. 2.1. In the experiments with stratification, strength in the range $0.28 \leq N \leq 0.8$ was used.

$$N = \sqrt{\frac{g}{\rho}\left|\frac{\partial \rho}{\partial z}\right|} \tag{2.1}$$

2.1.3 Body

The bodies used are small models shown in Fig. 2.6 capable of self-propulsion in either direction with twin-propellers. Of the two models used in experiments, the

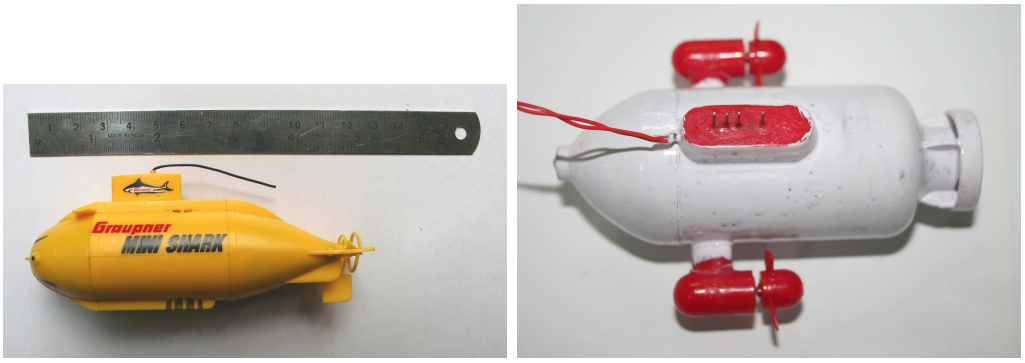

(a) (b)

Figure 2.6: Model submarines used as self-propelled bodies

first model had a diameter of 35 mm and a length of 125 mm. The second model had a body diameter of 36 mm, was 100 mm long and had a propeller radius of 10 mm. The first model was used to simulate a bluff body with its propellers off. The second model was modified to be externally powered for better control over the angular velocity of the propellers. The propellers' speed in revolutions per second was calibrated underwater using an optical interruptor circuit. The propellers were capable of rotational speeds from 50 to 100 revolutions per second.

2.2 Flow visualization

Data acquired from the experiments were in the form of flow visualizations. Multiple cameras (a digital SLR, and a video recorder) were used to capture information appropriately.

Flow visualization was performed employing a variety of techniques each with its own advantages and disadvantages. A short description of the methods employed is provided.

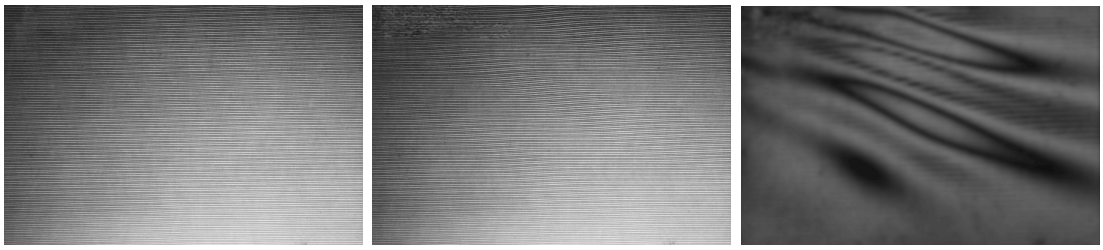

(a) Reference (b) Subject (c) Difference

Figure 2.7: A demonstration of Synthetic Schlieren. The reference image is the undisturbed flow field. When this image is digitally subtracted from an image with a flow of our interest, we obtain an image with all but the flow of interest removed.

2.2.1 PLIF

Planar Laser Induced Fluorescence, as the name implies, is essentially a laser sheet lit by fluorescent dye in the flow field. For our experiments, the dye, Rhodamine 6G, was used in conjunction with an Nd-YAG pulsed laser at 532nm. The technique gives us near-instantaneous flow fields (due to the 5ns pulse duration) in a specific plane of interest. The technique was primarily used to visualize flow in a propelled jet.

2.2.2 Synthetic Schlieren

Synthetic Schlieren or Background Oriented Sclieren, is a technique where changes in the density field are captured by comparing the images of a background with the reference state. As shown in Fig. 2.7 the reference image is digitally subtracted from the subject image and the difference image is smoothened, enhanced and presented. The method however has an integrated effect over the depth of the medium. It has the advantage of being an optically non-intrusive technique and unlike dye-based techniques where the tank is rendered unusable due to accumulated dye more number of experiments can be conducted with this visualization.

2.2.3 Dye injection

Visualization by dye injection using $KMnO_4$ was used extensively, especially in the testing phases of different experiments. The dye in all experiments (including PLIF) had to be density matched with the surrounding medium to prevent it from rising or sinking from the intended plane of visualization. A denser dye (this happens when the surrounding fluid is just water) was made lighter by adding acetone and the lighter dye was made denser with brine.

The dye injection setup was integrated with the moving carriage which allowed us to use these visualization methods even when the body is towed. The dye reservoir was attached to the carriage. A tube carrying the dye from the reservoir to the model was carefully taped to the leading edge of the sting to preserve its streamlining effect. The dye is gravity driven. In the case of the wake visualization, the dye ($KMnO_4$) was allowed to seep from the nose of the model, which then flows along the side-walls of the model and defines its wake. With the propelled jet experiments (using 0.05% w/v Rhodamine 6G with PLIF), the ends of two dye tubes were positioned right in front of the propellers so they would be sucked in and evenly distributed into the jet by turbulent mixing.

2.3 Observations

2.3.1 Towed bluff body

The first set of experiments involved towing a bluff body (the yellow model with propellers turned off) at a constant speed. The image in Fig. 2.8 was from the test run performed in a stratified medium of $Fr \approx 0.8$ by towing the body at 2 cm/s giving an $Re \approx 700$. The flattened 'pancake' vortex shedding is evident in

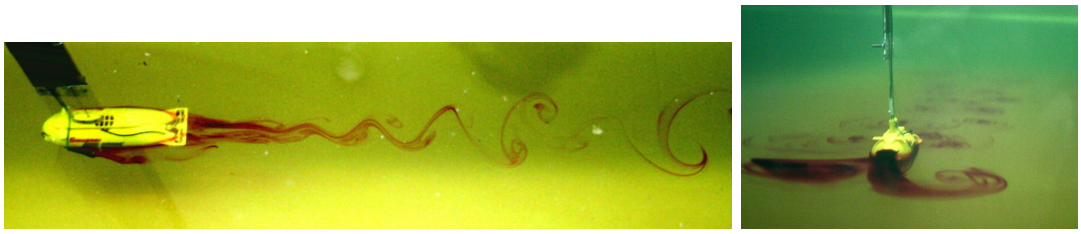

(a) Top view (b) Side view

Figure 2.8: Bluff body wake in a stratified flow showing quasi two-dimensional vortex shedding

Fig. 2.8b.

2.3.2 Wake difference between stratified and unstratified cases

Case 1: $Fr = \infty$, $Re = 700$, $N = 0$

In figures 2.9 and 2.10 the wake of a towed bluff body in a homogeneous medium is shown at different time intervals. The wake is three-dimensional and due to the high dissipation and mixing in a homogeneous medium, after $1800s$ the wake is hardly visible.

Case 2: $Fr = 2$, $Re = 700$, $N = 0.28$

In figures 2.11 and 2.12 the wake of a towed bluff body in a stratified medium with $Fr = 2$ is shown at different time intervals. The vortex shedding is very irregular and asymmetric but still restricted to its density plane and after $1800s$ the coherent vortex pancakes are still seen.

Case 3: $Fr = 1$, $Re = 612$, $N = 0.5$

In figures 2.13 and 2.14 the wake of a towed bluff body in a stratified medium with $Fr = 1$ is shown at different time intervals. The vortex shedding is not

as irregular as in the previous case of $Fr = 2$. After $1800s$ the coherent vortex pancakes are clearly seen.

Summary

We observe that in a stratified medium, mixing and vertical velocity in the wake are suppressed. This quasi two-dimensionalization also leads to a long lasting tracer signature.

2.3.3 Propelled jet

Here the body was kept stationary and the propellers of the body were run at different speeds. A stratification of $N = 0.8$ was established for the following experiments. The propelled jet thus produced was visualized primarily using PLIF (planar laser induced fluorescence). The Reynolds number based on the propeller tip speed and its radius is given by Eqn. 2.2. The Froude number given by Eqn. 2.3 increases proportionally with Re as the velocity scale is common to both non-dimensional numbers.

$$Re_{prop} = \frac{U_{tip} R_{prop}}{\nu} \tag{2.2}$$

$$Fr_{prop} = \frac{U_{tip}}{N R_{prop}} \tag{2.3}$$

Case 1: Vertical section

In Figs. 2.15, 2.16 and 2.17, we have presented the vertical sections of the jet captured using PLIF and Synthetic Schlieren techniques. The increase in vertical wake height and the distance of the maximum wake height location with the Reynolds number is evident. In Fig. 2.17 we also observe the generation on internal

gravity waves from the collapsing wake. These waves can reach the surface even when the turbulent wake itself cannot.

Case 2: Horizontal section

In figure 2.18 we have horizontal mid-plane sections of the jet. At low rps, the turbulent jet is seen but at higher rps, we notice two phenomena. The first is the strong interaction of the back-flow with the expanding jet and the second is the relative quiescence in the turbulence levels. This seems to indicate that at high rps most of the turbulent flow happens out of the mid-plane.

Case 3: Transverse sections at Re = 38080 (26.7 rps)

In Fig. 2.19 we have the body slowly towed (at 1 cm/s) with the propellers switched on to obtain transverse sections of the propelled jet. The Reynolds number of the wake due to towing is much smaller than that of the jet and does not influence the jet much. The interaction of the jet with back-flow however is not known. From the images, we notice that close to the propellers the jet expands into the upper and lower planes more and is not axisymmetric. Moving away from the propellers, the jet is seen to slowly collapse and simultaneously expand along the horizontal mid-plane.

2.3.4 Surface effects

Case 1: Surface streaks

In Fig. 2.20 we have documented the effect of the switching the jet on and off affecting the surface. The surface of water behind the propellers is sprinkled with white powder to act as surface tracers. Fig. 2.20a represents the surface before the

propellers are switched on. Once the propellers are switched on, the second image shown in fig. 2.20b is taken with an exposure of 30 seconds. The image shows that the entire surface has moved towards the propellers rather than away during this time. Fig. 2.20c is the third image captured once the surface stops moving any more with the propellers still switched on. When the propellers are switched off and another image captured as shown in fig. 2.20d the surface has moved back to its initial position before the experiment was begun.

Case 2: Tracking the layer just below the surface (approx 2cm deep)

In figures 2.21 and 2.22, we capture the effects of the propelled jet not at the surface but a couple of centimeters below it. Dye is introduced at the layer where the stratification just begins by careful density matching. With the propellers switched on, we notice how this entire plane is pulled towards the propellers rather than away. The velocity observed in this case is quite large and continuous, which suggests that this may be due to entrainment from the jet. The slow fading of the dye also suggests that the flow here is not turbulent but is experiencing shear. Once the propellers are switched off, the flow relaxes back a little but is irreversible unlike what we observed on the surface.

2.3.5 Vertical velocity profile of a propelled jet

This experiment is performed at $Re = 38080$ or $26.7rps$. The velocity profile across the propelled jet is visualized as the vertical (more or less) dye-lines created get sheared as the propeller is started and the jet is slowly established (2.23 and 2.24). $N = 0.8$ for this experiment. This experiment was devised to better understand the observations made with the last two experiments and from the images we see that the idea we had built up with the previous observations are indeed true. The

turbulent jet is restricted to a few propeller heights but the entrainment creates a reverse flow. The reverse flow velocities increase with the proximity to the jet.

2.4 Discussion

Wakes observed here behave as described in literature. A wake in stratified flow at low Froude numbers produces pancake like vortices. The symmetry of the vortex shedding increases with smaller Froude numbers. When compared to a wake in a homogeneous medium, stratified wakes are more persistent and are restricted to their density layer.

A propelled jet is a interesting case which hasnt been studied as widely. The collapse of the expanding jet creates internal gravity waves which offer a chance of being detected on the surface but the amplitude of the surface disturbance they would create is not known. The jet itself expands vertically to a few propeller radii and indefinitely in the horizontal plane.

The plots in 2.25 mostly show that all length scales, maximum vertical jet width, location of the maximum jet width and the jet width far downstream (38 propeller radii) increase with the Reynolds number. The exact relationship with the Reynolds number however would need data from a much larger range of Reynolds numbers.

The effect of entrainment as seen by the sub-surface dye-lines and vertical dye-lines is a new observation. The stratification plays a large role in determining the nature of entrainment. Most of the entrainment due to turbulent mixing happens close to the vertically expanding section of the jet as shown in Fig. 2.25a. This region appears like a sink-hole where all the dye from the top layers are sucked down. After the maximum vertical jet width, there is very little mixing and we

observe only shear. The effect of the finite tank on the backflow also cannot be ignored. More experiments with a smaller jet may shed light on the effects of stratification on the backflow due to entrainment. If the backflow in the vertical velocity is due to entrainment and not due to the finite tank, then this may explain the observation shown in Fig. 1.1 and reported by Sheres & Munk (1992).

With regard to the surface streaks, the phenomenon does not show continuous deformation suggesting that this may be a simple readjustment of the surface to the effect of switching the propellers on in a finite tank. As the propellers push back fluid, the horizontally expanding jet and the stratification prevent backflow. We speculate that this could cause the surface levels behind the propellers to increase and dip in front of the propellers causing the surface to slide towards the propellers. Once the propellers are switched off, the surface levels drop back to normal and thus slide back into the initial position.

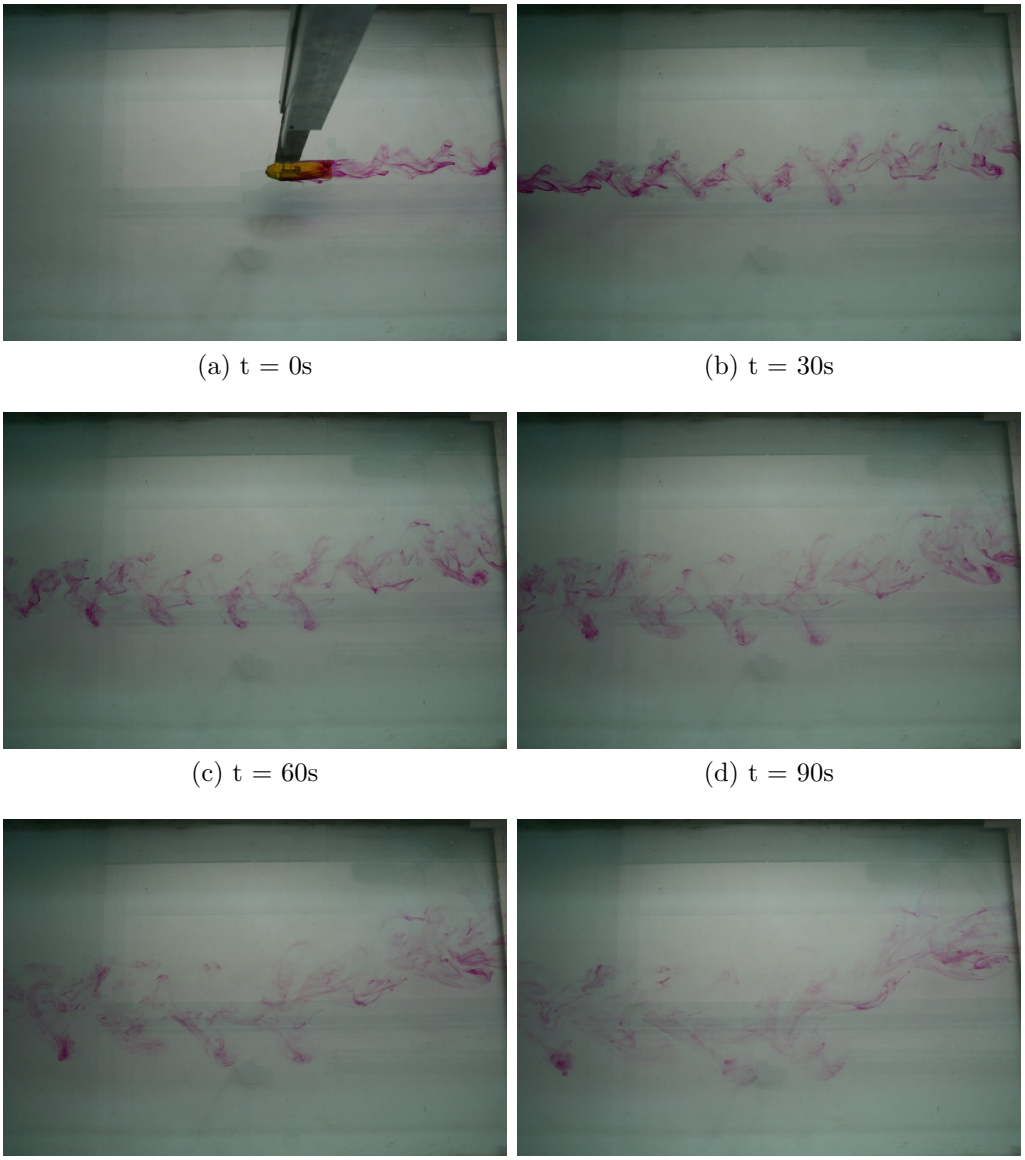

(a) t = 0s (b) t = 30s

(c) t = 60s (d) t = 90s

(e) t = 120s (f) t = 180s

Figure 2.9: Wake visualization at $Re = 700$ and $Fr = \infty$ from 0 to 180 seconds

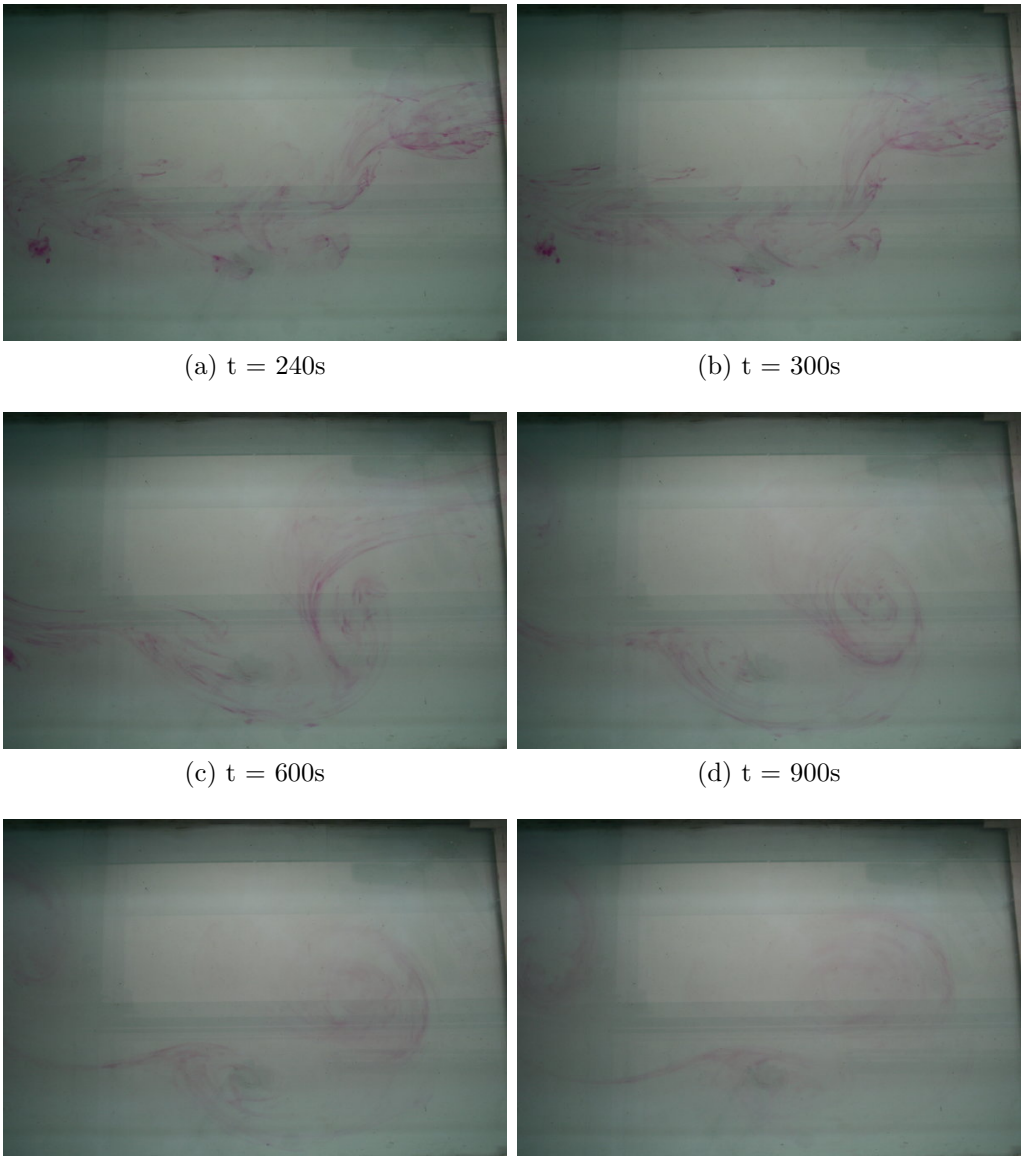

(a) t = 240s (b) t = 300s

(c) t = 600s (d) t = 900s

(e) t = 1200s (f) t = 1800s

Figure 2.10: Wake visualization at $Re = 700$ and $Fr = \infty$ from 240 to 1800 seconds

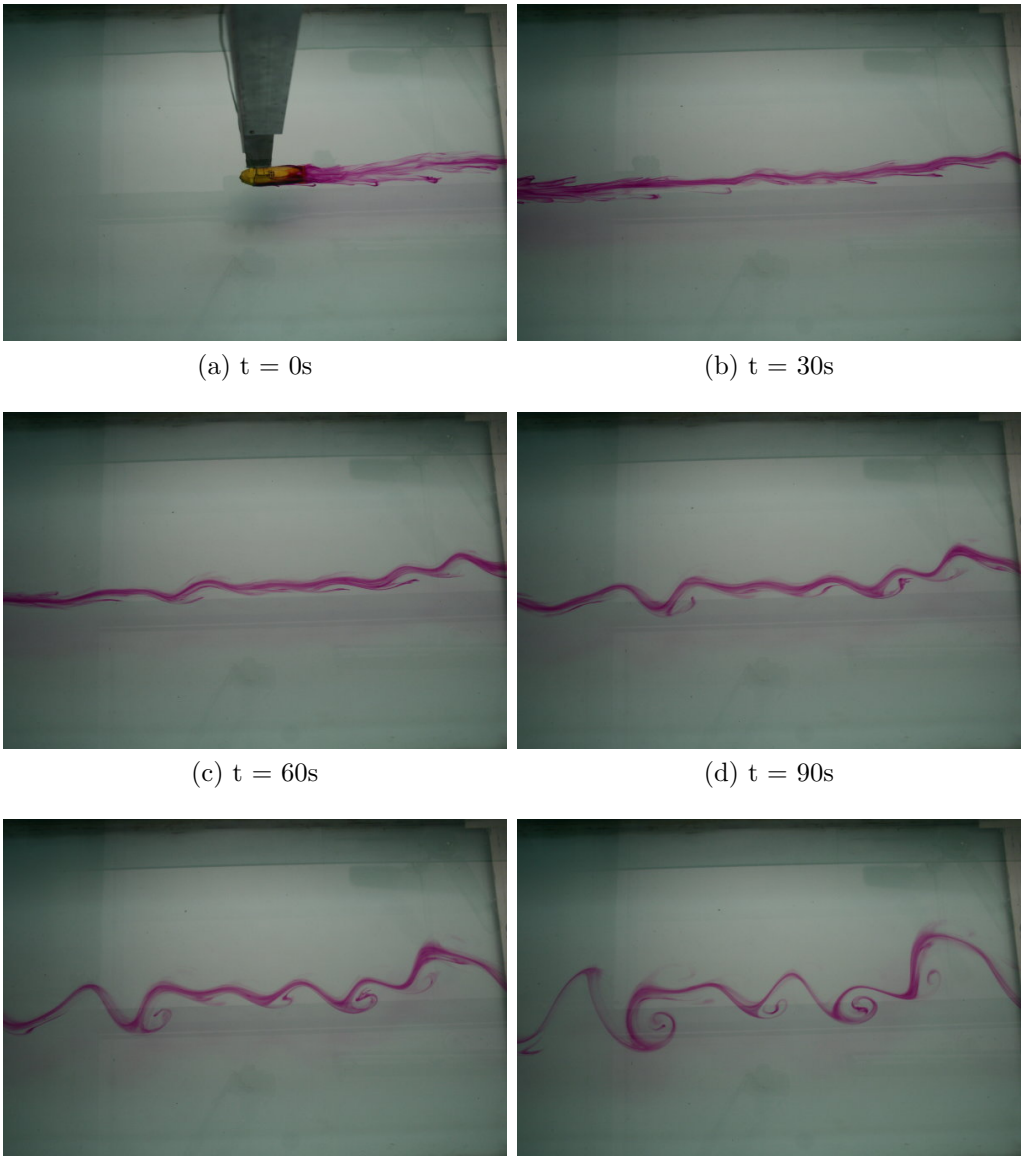

(a) t = 0s (b) t = 30s

(c) t = 60s (d) t = 90s

(e) t = 120s (f) t = 180s

Figure 2.11: Wake visualization at $Re = 700$ and $Fr = 2$ from 0 to 180 seconds

(a) t = 240s (b) t = 300s

(c) t = 600s (d) t = 900s

(e) t = 1200s (f) t = 1800s

Figure 2.12: Wake visualization at $Re = 700$ and $Fr = 2$ from 240 to 1800 seconds

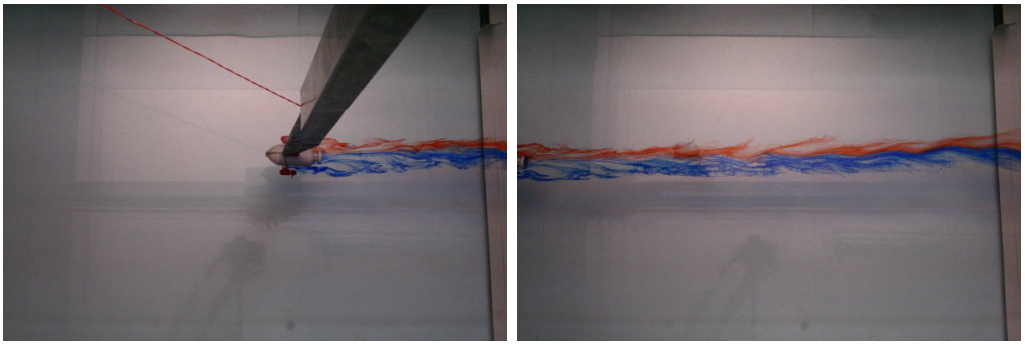

(a) t = 0s (b) t = 30s

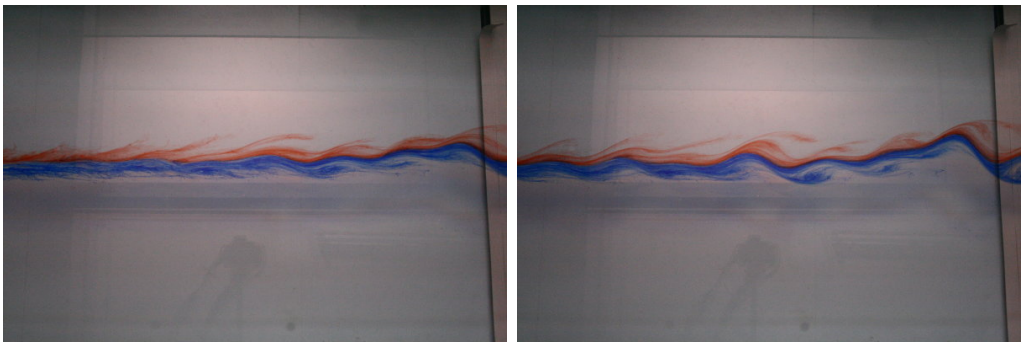

(c) t = 60s (d) t = 90s

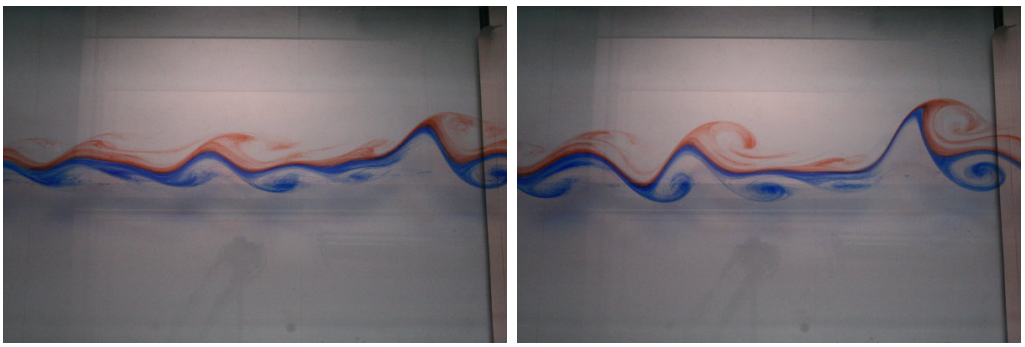

(e) t = 120s (f) t = 180s

Figure 2.13: Wake visualization at $Re = 612$ and $Fr = 1$ from 0 to 180 seconds

(a) t = 240s (b) t = 300s

(c) t = 600s (d) t = 900s

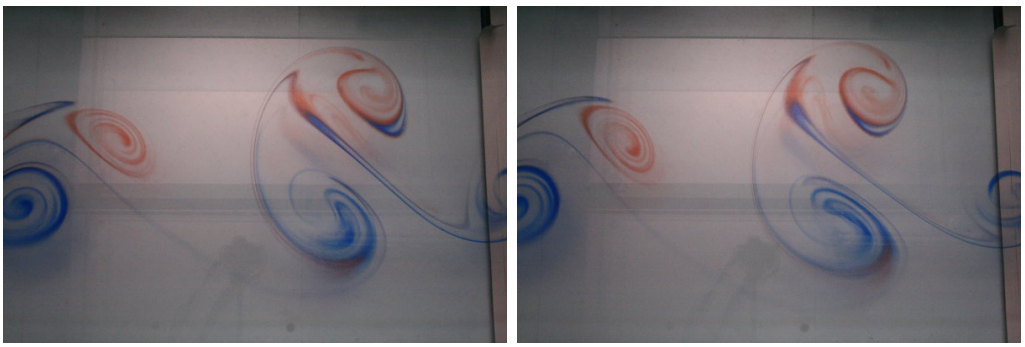

(e) t = 1200s (f) t = 1800s

Figure 2.14: Wake visualization at $Re = 612$ and $Fr = 1$ from 240 to 1800 seconds

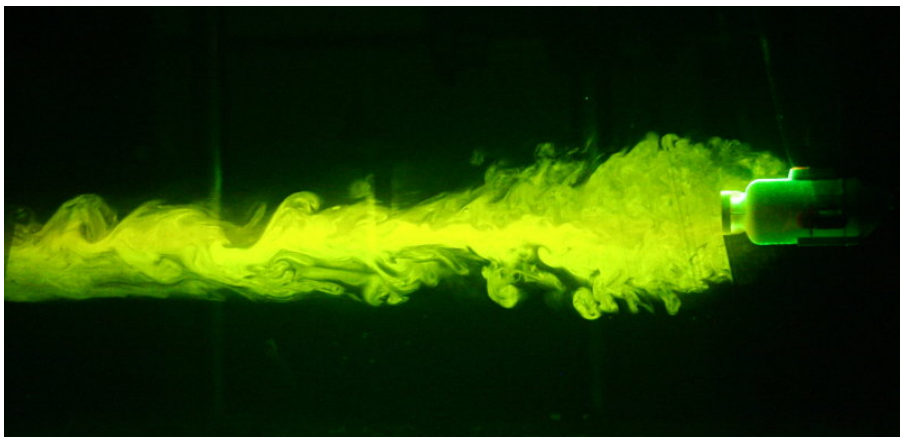

(a) 16.7 rps

(b) 20.0 rps

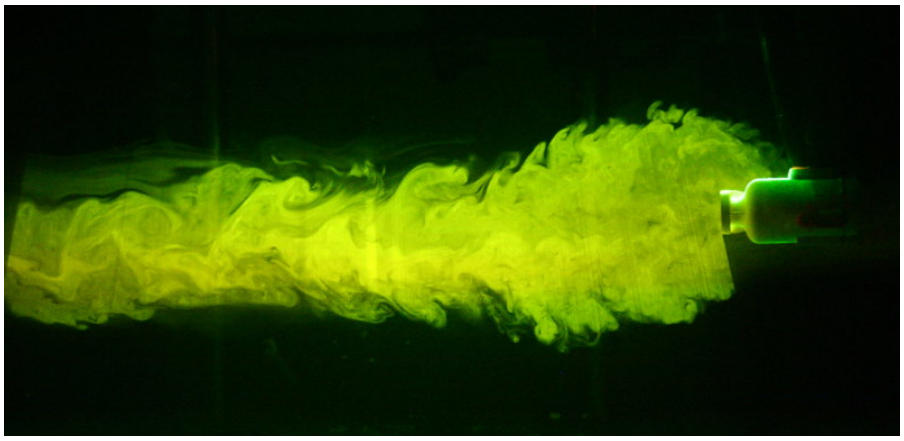

(c) 23.3 rps

Figure 2.15: PLIF: Propelled jet vertical cross sections from 16.7 to 23.3 propeller rps

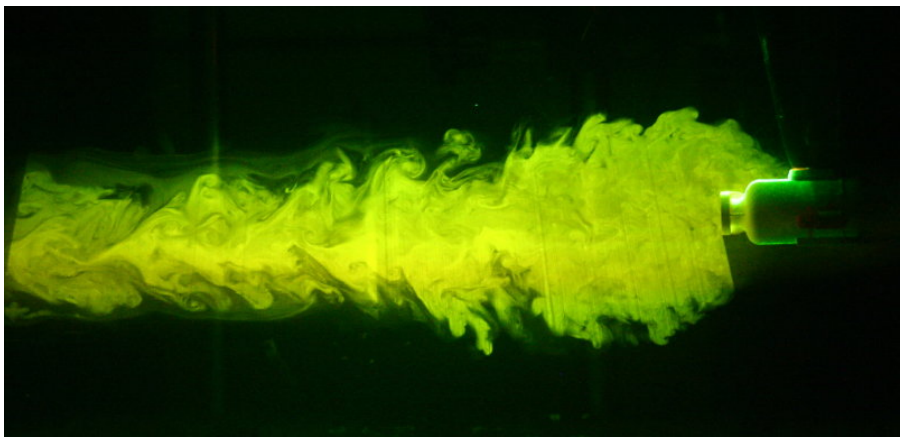

(a) 26.7 rps

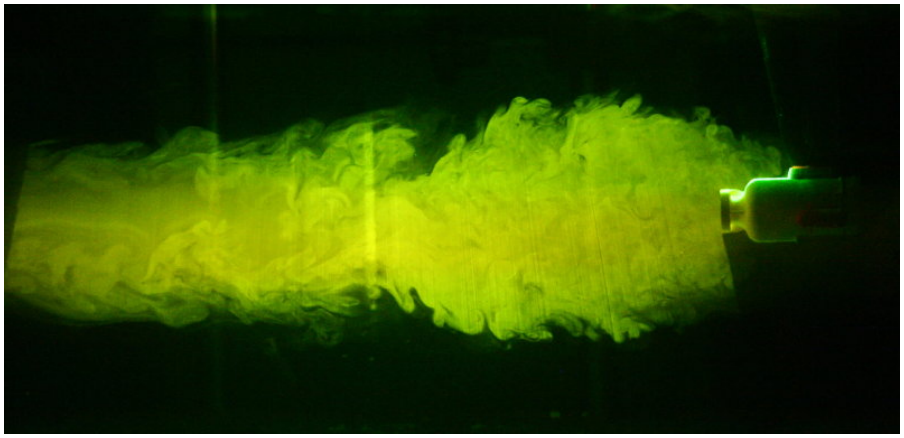

(b) 30.0 rps

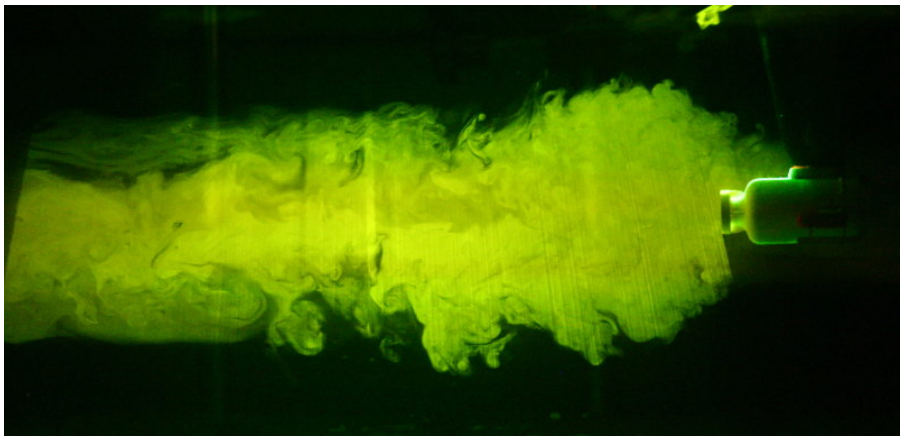

(c) 33.3 rps

Figure 2.16: PLIF: Propelled jet vertical cross sections from 26.7 to 33.3 propeller rps

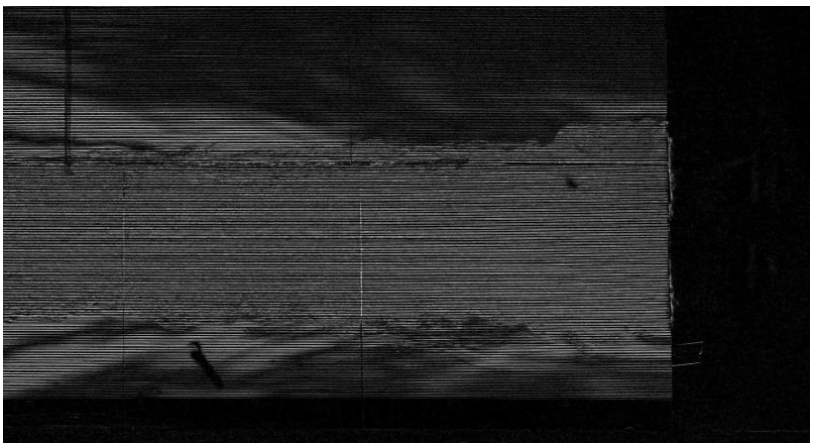

(a) 20.0 rps

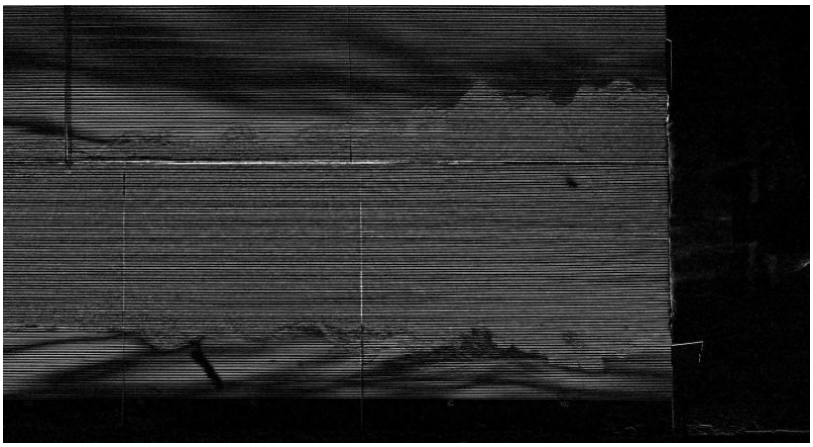

(b) 26.7 rps

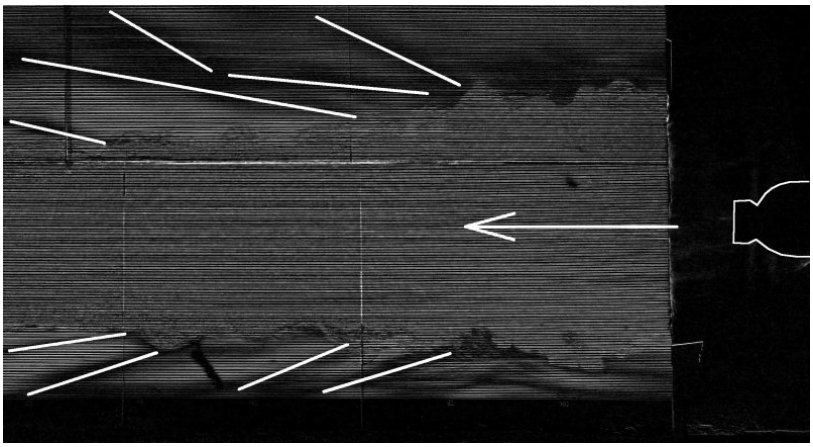

(c) 26.7 rps with body and internal waves highlighted

Figure 2.17: Schlieren: Propelled jet vertical cross sections for (a) 20.0 and (b) 26.7 rps. (c) The model and internal gravity waves in case (b) are outlined for clarity

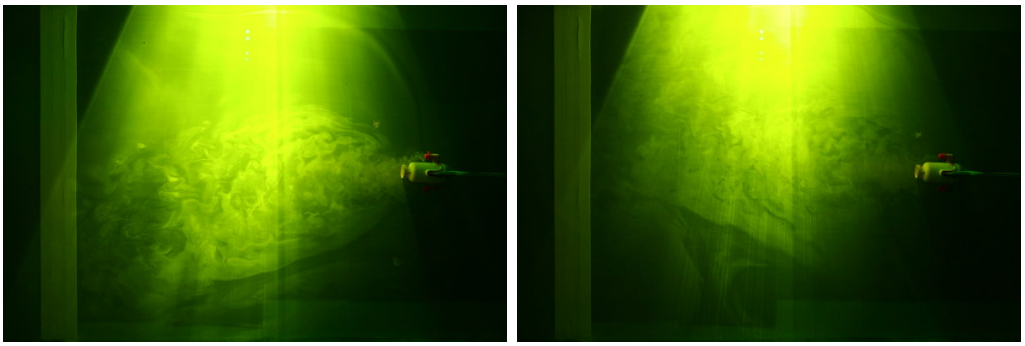

(a) 16.7 rps

(b) 20.0 rps

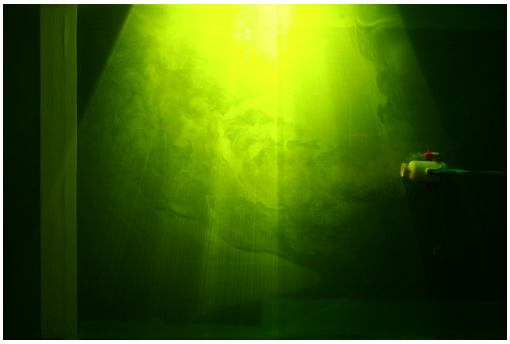

(c) 23.3 rps

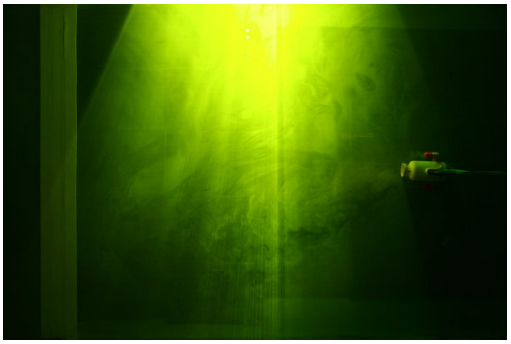

(d) 26.7 rps

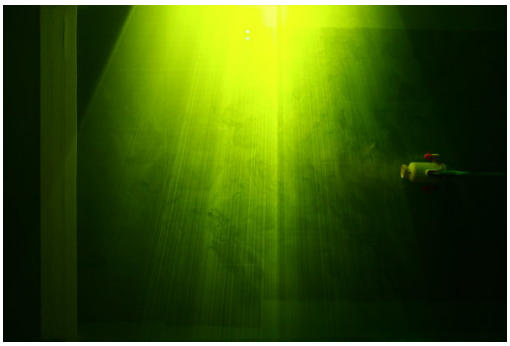

(e) 30.0 rps

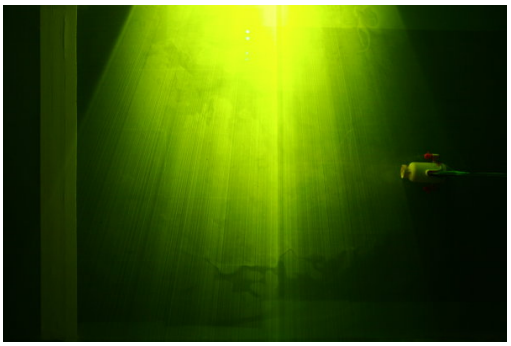

(f) 33.3 rps

Figure 2.18: PLIF: Propelled jet horizontal plane visualization from 16.7 to 33.3 rps

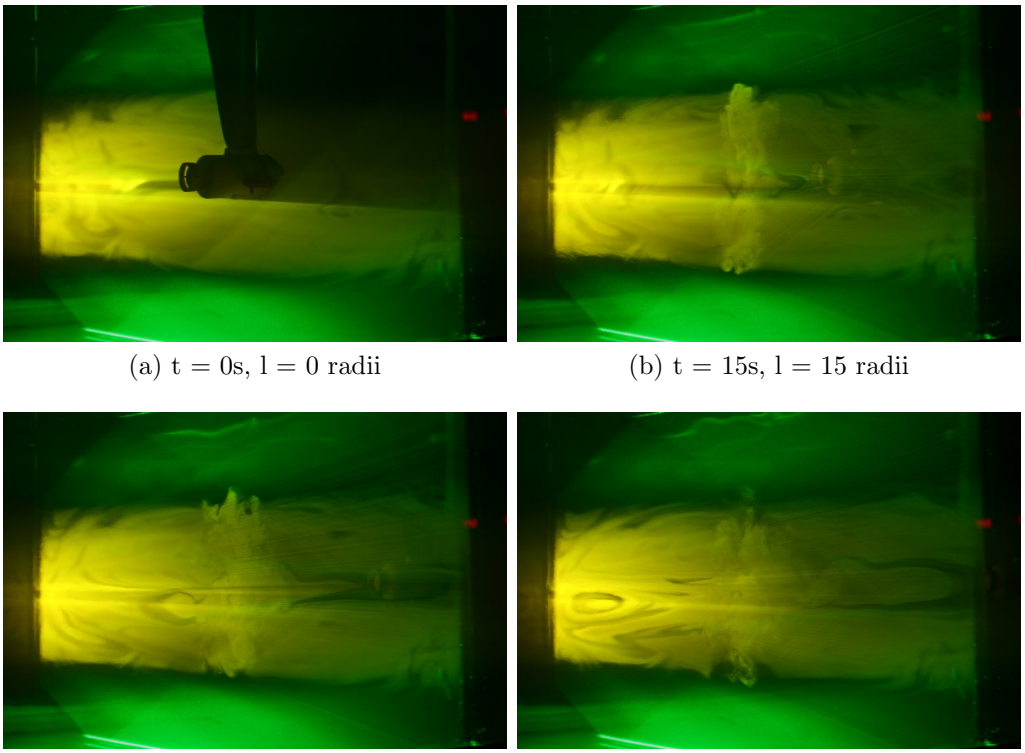

(a) t = 0s, l = 0 radii (b) t = 15s, l = 15 radii

(c) t = 25s, l = 25 radii (d) t = 40s, l = 40 radii

Figure 2.19: PLIF: Propelled jet transverse plane visualization with elapsed time and location downstream in units of propeller radii

(a) Initial state at t = 0s

(b) 30 second exposure photo as the jet is switched on at t = 11s

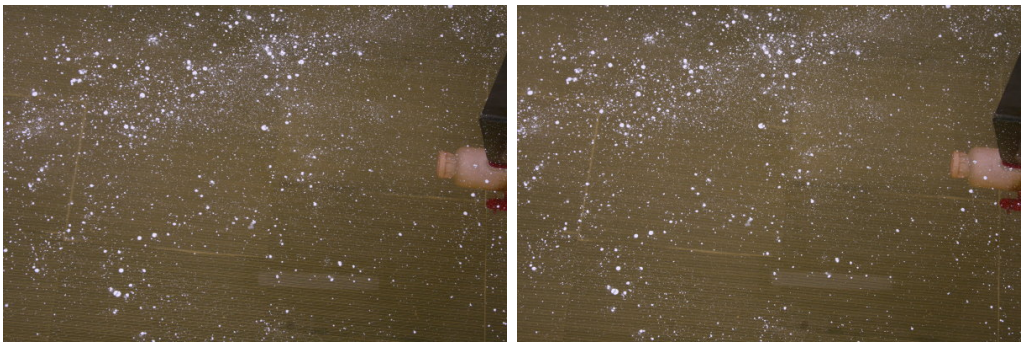

(c) Final state at t = 55s

(d) Jet is switched off and at t = 189s the surface is back to its Initial state

Figure 2.20: Long exposure photos of the surface sprinkled with white powder as the jet is switched on and off. The sprinkled surface readjusts by a few millimeters when the propellers are switched on and after the propellers are switched off it moves back to its initial state.

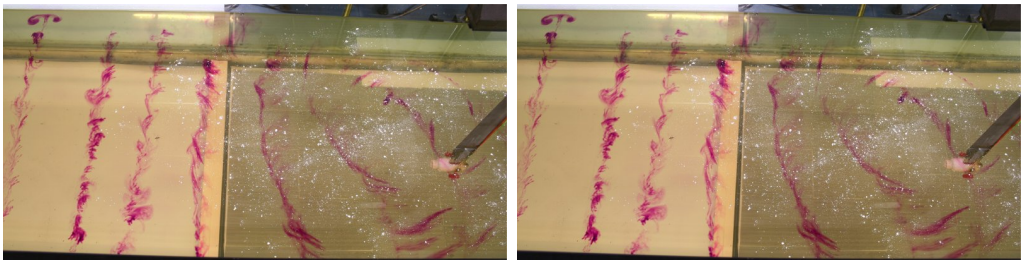

(a) t = 0s (b) t = 6s

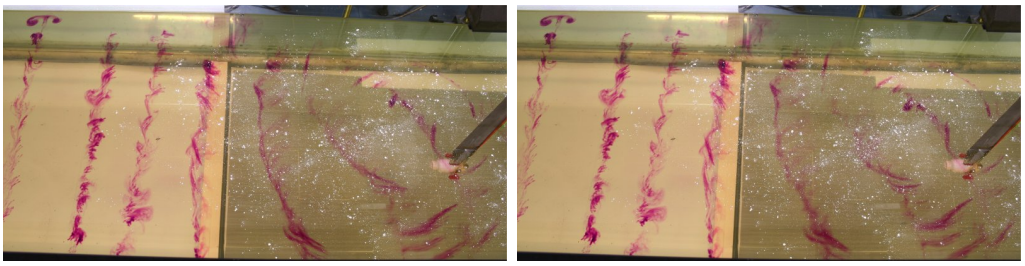

(c) t = 11s (d) t = 17s

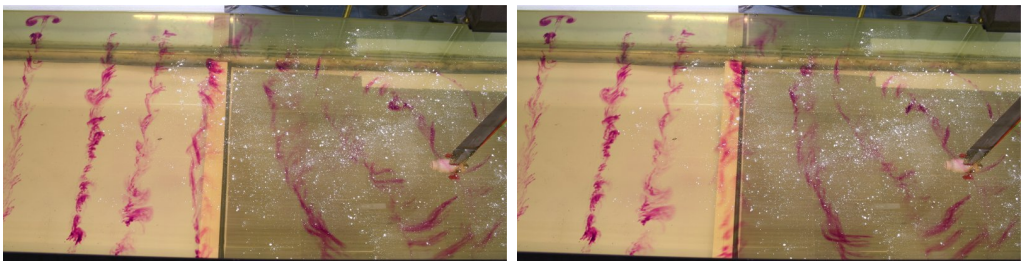

(e) t = 22s (f) t = 28s

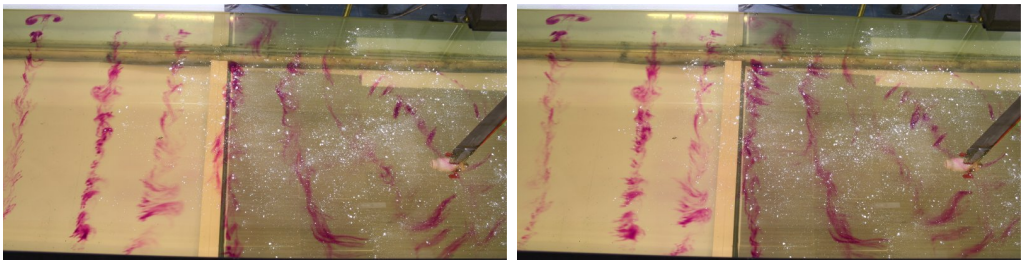

(g) t = 34s (h) t = 45s

Figure 2.21: Tracking the dye layer just below the surface when the jet is switched on at t = 0s

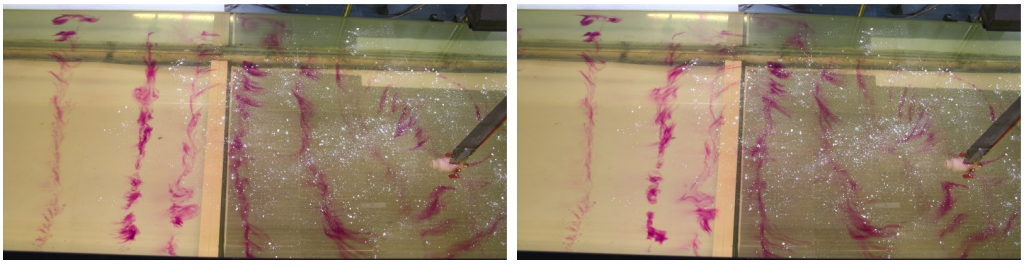

(a) t = 55s (b) t = 65s

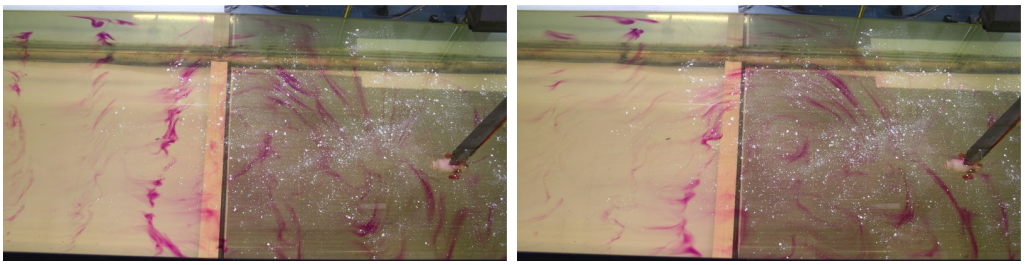

(c) t = 91s (d) t = 120s (jet is switched off now)

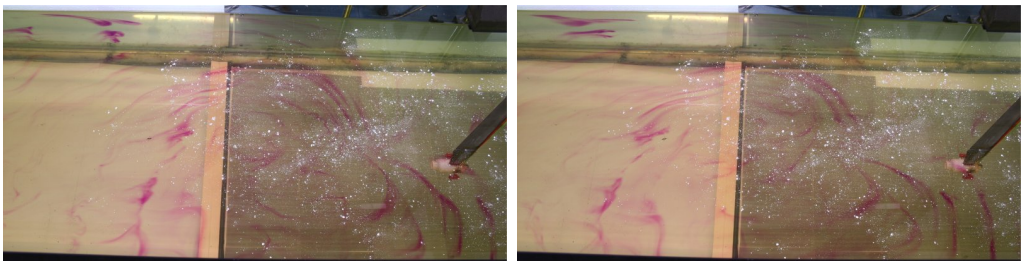

(e) t = 141s (f) t = 161s

(g) t = 181s (h) t = 220s

Figure 2.22: Tracking the dye layer just below the surface when the jet is switched on at t = 0s. The jet is switched off at t = 120s

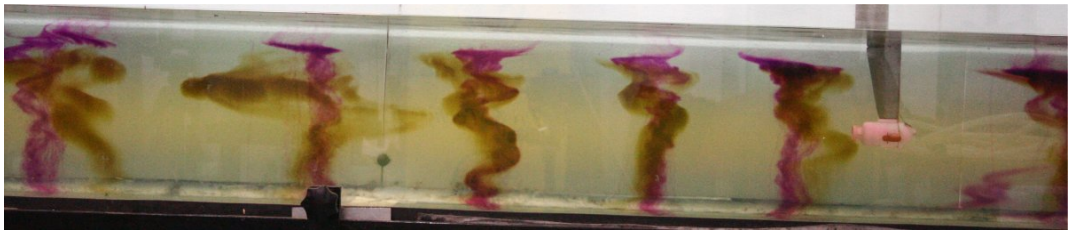

(a) t = 0s

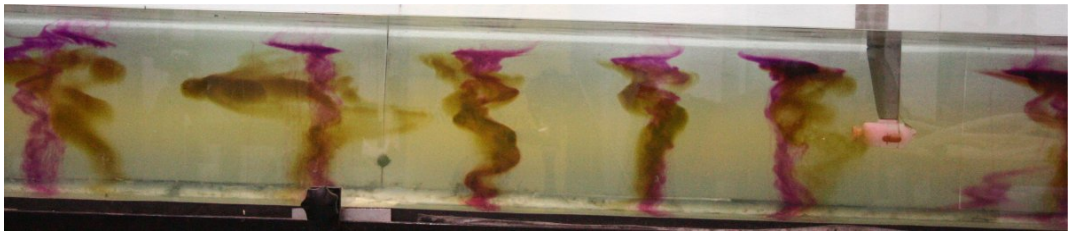

(b) t = 5s

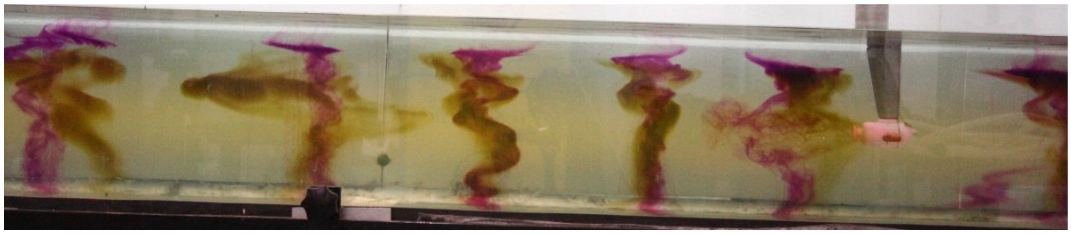

(c) t = 10s

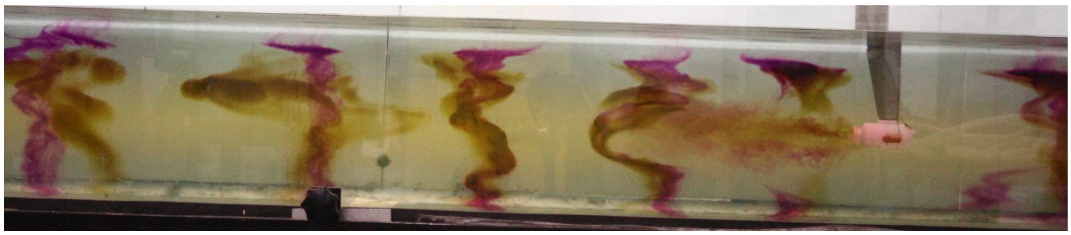

(d) t = 20s

(e) t = 35s

Figure 2.23: Propelled jet vertical plane visualization

(a) t = 50s

(b) t = 75s

(c) t = 100s

(d) t = 125s

(e) t = 150s

Figure 2.24: Propelled jet vertical plane visualization

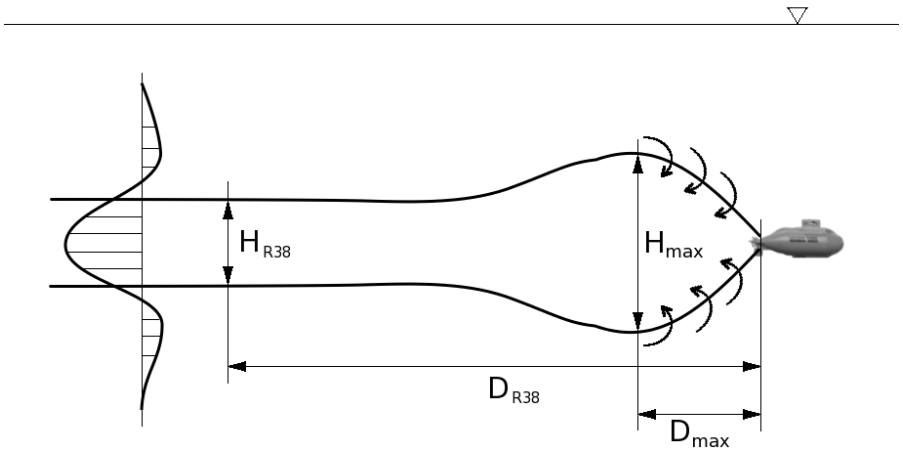

(a) Schematic of the vertical cross-section of a propelled jet. The maximum vertical jet width is H_{max} and D_{max} the location of the maximum vertical jet width. At 38 propeller radii downstream, D_{R38}, the vertical jet width is given by H_{R38}.

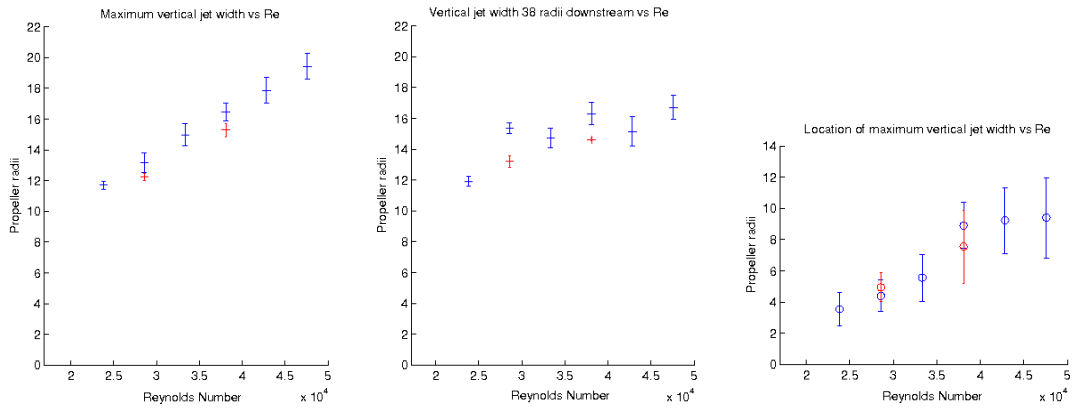

(b) Maximum vertical jet width

(c) Vertical jet width 38 propeller radii lengths downstream of the propeller

(d) Location of maximum jet width w.r.t. the propeller

Figure 2.25: Propelled jet data (blue data points are from PLIF and red data points from Synthetic Schlieren)

CHAPTER 3

NUMERICAL SIMULATIONS

3.1 Introduction

To study the behaviour of the decay of wakes left by a self-propelled body a numerical simulation of the flow in two-dimensions was performed to better understand the wake-jet combination in the flow behind such a body. A novel minimal model of a self-propelled body was constructed in the process and the data obtained from the simulations is presented in this chapter.

3.2 Discrete Vortex Methods

Discrete vortex method is a particle based method where the flow is described completely by vortex particles. The idea is mathematically sound and results from the vorticity-streamfunction formulation of the Navier-Stokes equation. It is a gridless scheme where the vorticity field is discretized into vortex 'blobs'. The blobs used in this work are essentially Gaussian kernels (a Lamb vortex) defined by a center and a core radius. Leonard (1980) summarizes the advantages and disadvantages posed by vortex methods:

- Vortex elements (which represent computational points) are required only in regions with vorticity but the number of operations per time step is proportional to the square of the number of vortex elements. This effect can however

be mitigated with the use of fast multipole methods.

- The Lagrangian approach allows small-scale features to be more accurately computed but smooth flows tend to be error prone.

- The boundary conditions at infinity are exactly solved for but the no-slip condition at walls pose a challenge.

3.2.1 Formulation

The governing equation is the vorticity formulation of the incompressible Navier-Stokes equations in two dimensions. In two dimensions the vortex stretching term vanishes giving (3.2) from the general vorticity transport equation (3.1).

$$\frac{\partial \boldsymbol{\omega}}{\partial t} + \boldsymbol{u} \cdot \nabla \boldsymbol{\omega} = \boldsymbol{\omega} \cdot \nabla \boldsymbol{u} + \nu \nabla^2 \boldsymbol{\omega} \tag{3.1}$$

$$\frac{D\boldsymbol{\omega}}{Dt} = \nu \nabla^2 \boldsymbol{\omega} \tag{3.2}$$

The advection and viscous diffusion operators can now be split and solved sequentially. In the advection step (3.3), the velocity, $\boldsymbol{u}(\boldsymbol{r}, t)$, at each vortex blobs center is given by the value of the velocity field at its location. This velocity can be evaluated using the Biot-Savart law and the vortex is displaced by $\boldsymbol{u}\Delta t$ where Δt is the time step.

$$\frac{D\boldsymbol{\omega}}{Dt} = 0 \tag{3.3}$$

$$\frac{d\boldsymbol{r}_i}{dt} = \boldsymbol{u}(\boldsymbol{r}_i, t) \tag{3.4}$$

The vorticity field is represented by the superposition of vortex blobs (3.5) where each blob is defined by a kernel. The kernel in (3.6) is a Lamb vortex.

$$\omega(\boldsymbol{r},t) = \sum_{i=1}^{N} \Gamma_i(t)\zeta_{\sigma_i}(\boldsymbol{r} - \boldsymbol{r}_i(t)) \tag{3.5}$$

$$\zeta_\sigma(\boldsymbol{r}) = \frac{1}{\pi\sigma^2} \exp\left(\frac{-|\boldsymbol{r}|^2}{\sigma^2}\right) \tag{3.6}$$

The Biot-Savart law can be represented by (3.7) and (3.8) for a generic kernel.

$$\boldsymbol{u}(\boldsymbol{r}_i,t) = \sum_{j=1}^{N} \Gamma_j(t) \frac{\hat{k} \times (|\boldsymbol{r}_i - \boldsymbol{r}_j(t)|)}{|\boldsymbol{r}_i - \boldsymbol{r}_j(t)|^2} F\left(|\boldsymbol{r}_i - \boldsymbol{r}_j(t)|\right) \tag{3.7}$$

$$F(y) = \int_{s=0}^{y} s\zeta(s)ds \tag{3.8}$$

For a Lamb vortex the function $F(y)$ reduces to (3.9).

$$F(|\boldsymbol{r}|) = \frac{1}{2\pi}\left[1 - \exp\left(\frac{-|\boldsymbol{r}|^2}{\sigma^2}\right)\right] \tag{3.9}$$

3.2.2 Viscous Schemes

Many different models have been proposed and used to accomplish the diffusion step. A few well known methods are the modified core expansion method by Rossi (1996), particle strength exchange by Mas-Gallic & Raviart (1987), diffusion velocity method by Ogami & Akamatsu (1991) and vorticity redistribution by Subramaniam (1996). Chorin (1973) applied random walk to the position of vortex blobs to statistically simulate diffusion. Some methods use hybrid schemes like the one proposed by Qian & Vezza (2001) where velocity evaluation alone is done using Biot-Savart and the vorticity diffusion and mass conservation taken care with finite

volume methods. Vortex-in-cell methods do just the opposite by using a grid to solve the Poisson equation for velocity evaluation and performing advection and diffusion using the Lagrangian approach

Core spreading and splitting

The method used in our work is the modified core-spreading method owing to its simplicity in coding and computational overhead. It is also purely gridless. The time-evolution of a lone lamb vortex can be exactly defined by a fixed center and a core-radius which increases with time given by the following relation:

$$\frac{d\sigma^2}{dt} = 4\nu \tag{3.10}$$

The same relation is used for the vortices in the core-spreading scheme. The linearity of the diffusion equation allows us to apply to the core-spreading to all blobs simultaneously in the flow field. Therefore, we have

$$\sigma_i^2(t + \delta t) = \sigma_i^2(t) + 4\nu\delta t \tag{3.11}$$

Unbounded core-spreading has however been shown to diverge from the Navier Stokes equation by Greengard (1985). Hence vortex blobs above a certain cut-off radius are split into multiple smaller vortex blobs. This modification was proposed and was proved to converge to the Navier-Stokes equations by Rossi (1996). The cut-off radius has been interpreted as an indicator of the spatial resolution of the simulation and we chose a cut-off radius accordingly.

In this work a higher-order splitting is used with one blob being split into one center blob and six off-center blobs as against splitting into four blobs. The zero,

first and second moments of vorticity are conserved during the split. To control the number of blobs in the problem form shooting up, following Subramaniam (1996), vortices of the same sign close to each other are merged together while conserving the zero and first moments of vorticity.

3.2.3 Boundary Conditions

The decaying nature of Gaussian vortex blob kernels means that the uniform flow field condition at infinity is automatically satisfied. The boundary conditions at a body surface however needs more light.

The body is discretized into N panels with a vortex blob in each panel. The vortex panel method is used to determine the circulation of each body vortex that satisfies the no-flow condition across the boundary. The system of equations however is singular since ensuring no-flow through N-1 panels would necessitate zero flux through the Nth panel for incompressible flow. Another condition exists in the form of the total circulation around the body. The circulation around the body and its wake is a conserved quantity and this can used as the Nth equation.

The vorticity on the body panels should be diffused into the flow and if solved correctly this should satisfy the no-slip condition. The magnitude of the rate of vorticity diffused depends on the normal gradient of vorticty at the surface (Sarkar (2004)). For a time step δt we can therefore represent the strength of the vortex sheet shed from the surface with (3.12)

$$\gamma(s) = -\nu \frac{\partial \omega}{\partial \hat{n}} \delta t \tag{3.12}$$

The diffused vorticity from each panel of length ℓ, given by $\ell\gamma(s)$, is converted into a vortex blob of equal circulation and core radius of the order of the panel length

and placed one core radius distance from the panel outside the body.

3.2.4 Force evaluation

The force on the body is evaluated by calculating the impulse(Saffman (1992)) imparted to the fluid by the vortex blobs. The change of impulse with time gives us the force exerted by the body on the fluid, F. This is equal and opposite to the force on the body.

$$I = \rho \int \boldsymbol{r} \times (\omega \hat{k}) dA \tag{3.13}$$

$$F = \frac{dI}{dt} \tag{3.14}$$

3.2.5 Variable core sizes based of local Re and higher order splitting

To optimize the number of blobs in the simulations, the concentration of blobs (and hence their core radii) in a given region can be based on the local Reynolds number. A scheme with spatially varying cores has been proven to converge to the Navier Stokes equation (Cottet *et al.* (2000)). The local Re was evaluated as the ratio of a blobs circulation to the kinematic viscosity. Though a crude model to start with, this method is grid-independent, has a scope for improvement and is very effective in controlling the number of vortices without losing much accuracy. The higher-order splitting scheme has already been indicated and offers an order of magnitude improvement over splitting into four blobs.

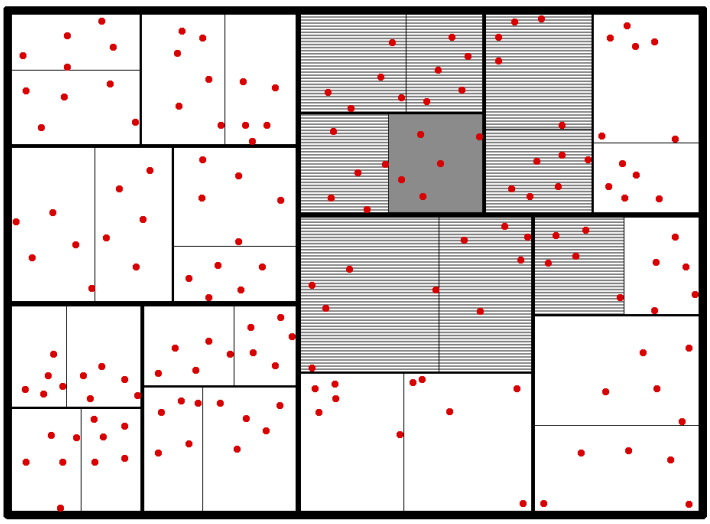

(a) Boxing algorithm schematic

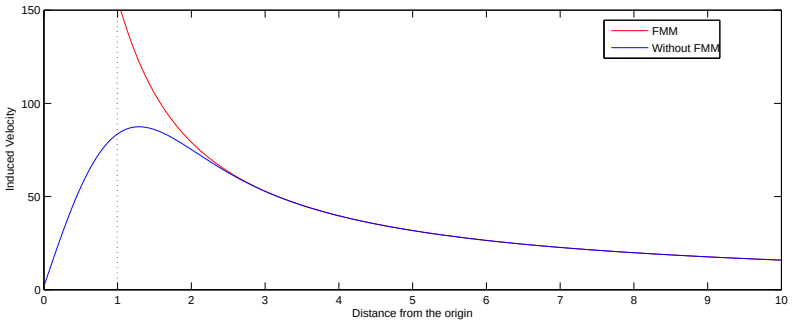

(b) Convergence of velocity evaluated by FMM

Figure 3.1: Fast multipole method for accelerating velocity evaluation

3.2.6 Fast Multipole Expansion

The velocity evaluation step is computationally intensive as it can involve $O(N^2)$ operations. A technique proposed by van Dommelen & Rundensteiner (1989) and its implementation by Clarke & Tutty (1994) called the zonal decompostion or summation algorithm is followed here. It involves lumping point vortices close together and writing a multipole expansion for the lump of vortices. The expansion is convergent above a cut-off radius from the center of the lump. A vortex above the

radius multiplied by a accuracy factor can be used for velocity evaluation. Since we use vortex blobs and not point vortices, we also ensure that the kernels of vortices in a multipole decay to converge to the velocity field of a point vortex. If not, direct summation is used. Thus vortices in the entire flow field are clubbed into multipoles as shown in Fig. 3.1a. To find the velocity at a particular vortex blob, one than resides in the box shaded grey in 3.1a, all multipoles far away from it to be convergent and accurate enough are used as an expansion and the rest of the blobs in hatched boxes that are too close are directly summed. The convergence of a multipole expansion to the exact expression for blobs placed inside a circle of one unit radius is shown in Fig. 3.1b. This scheme can involve at best $O(NlogN)$ operations and is of great benefit when the number of vortices exceeds a thousand. It should be noted that Greengard & Rokhlin (1997) have proposed an algorithm with $O(N)$ scaling. The method is not limited to Gaussian kernels and Draghicescu & Draghicescu (1995) have shown that a fast algorithm can be developed for any decaying kernel in two or three dimensions using Taylor expansion.

3.3 Validation

In this section, to verify if the method yields usable solutions, we simulate two test cases.

3.3.1 Circular Cylinder

The first test performed was the flow over a circular cylinder with $60 \leq Re \leq 160$. The Strouhal number of the cylinder's wake was obtained and compared with experimental results from Williamson (1988).

Fig. 3.2 shows the vorticity contour of the wake of a cylinder with $Re = 160$.

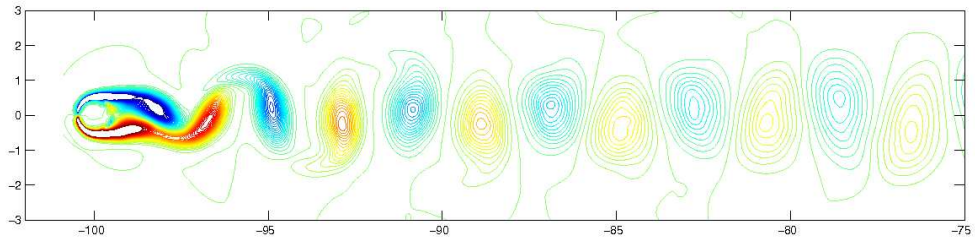

Figure 3.2: Vorticity contour of flow across a circular cylinder with $Re = 160$ at $t = 100$

A simulation for each Reynolds number in Fig. 3.3 was performed for $t = 100$ time units. Vorticity at a location two diameters downstream of the cylinder was monitored as shown in Fig. 3.3a and the Strouhal number was arrived from the Fast Fourier transform of this data. Fig. 3.3 shows a consistent overprediction of the Strouhal number by the simulations.

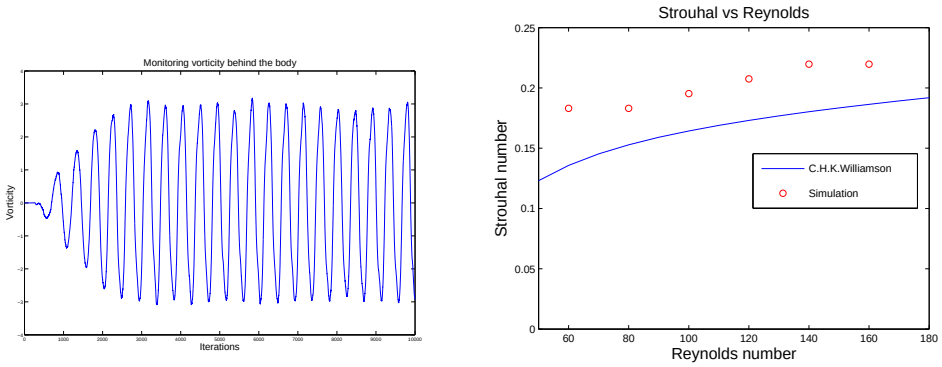

(a) Vorticity at a point two diameters behind the cylinder

(b) Strouhal number vs Reynolds number as obtained from the simulations

Figure 3.3: Flow across a circular cylinder

3.3.2 Vortex Merger

In the second test, two like vortices are allowed to merge into each other as shown in Fig. 3.4. The vortices have equal circulation, Γ, initial core radius, a_0, and are separated by a distance, b_0. The Reynolds number for this flow is defined as

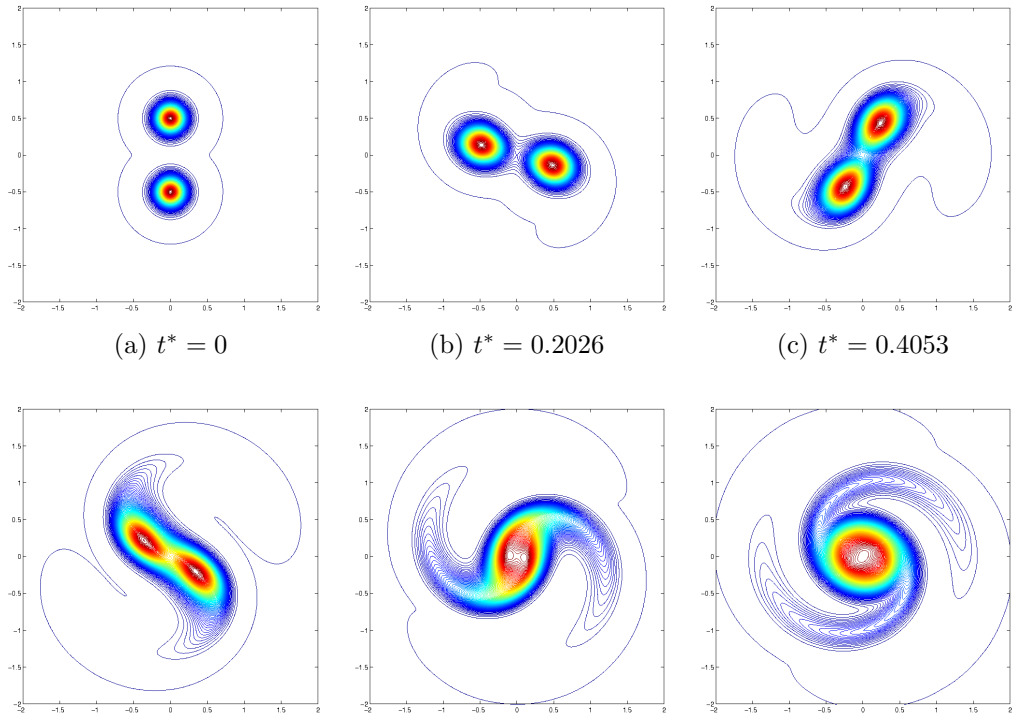

(a) $t^* = 0$ (b) $t^* = 0.2026$ (c) $t^* = 0.4053$

(d) $t^* = 0.6079$ (e) $t^* = 0.8106$ (f) $t^* = 1.0132$

Figure 3.4: Merger of two co-rotating vortices with $Re = 1000$

Γ_0/ν. The separation distance of the vortex centers with time was extracted and compared with the results of Brandt & Nomura (2006) in Fig. 3.5. The discrete vortex method performs better in this test. The intial geometry defined by the aspect ratio, a_0/b_0, was 0.177. The non-dimensional separation distance is defined as $b^* = b/b_0$ and the non-dimensional time as $t^* = t/T$ where $T = 2\pi^2 b_0^2/\Gamma_0$. The number of vortex kernels to start the simulation in Fig. 3.4a was 2 and reached $8,284$ in Fig. 3.4f.

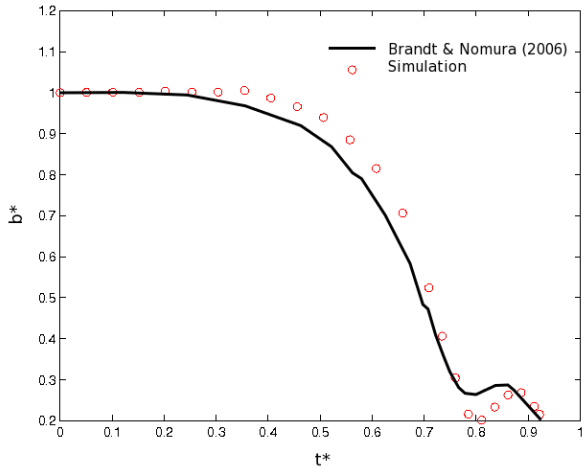

Figure 3.5: Comparison of vortex core separation versus time

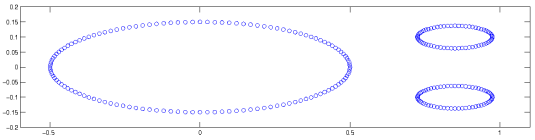

Figure 3.6: Geometry of the propulsive model

3.4 Propulsive body

3.4.1 Model description

A minimal model of a self-propelled body is constructed as shown in Fig. 3.6. It consists of an elliptic hull streamlined with the flow and two smaller ellipses. The hull has a fixed wall and contributes to the drag of the body. The two smaller ellipses right behind and on each side of the hull have moving walls.The circulation around the smaller ellipses is fixed by the user and hence they act like rollers, however they are set in opposite directions. This rolling coupled with vorticity diffusion creates a jet as illustrated in Fig. 3.7. This jet propels the body forward and is matched by the drag of the entire body and its acceleration. At steady state

the jets thrust equals the body drag. The control over the circulation of the rollers gives the user the freedom to perform various straight line maneouvers with the body.

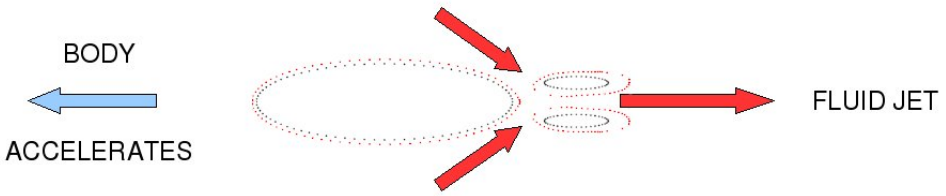

Figure 3.7: Schematic of model producing thrust and accelerating

3.4.2 Simulation plots

The data from simulation of the model propulsive body is presented in this section. Fig. 3.8 shows the vortex blob locations and the corresponding vorticity contour for the model towed at a unit velocity of 1 from right to left at $t = 20$ units. The same towed model at different time units is shown in Fig. 3.9. We can see the wake slowly developing as the body is towed impulsively at $t = 0$ and also observe the slow decay of the late wake at longer times.

Figures 3.10 and 3.11 are the plots of the model self-propelling from zero velocity. These images in Fig. 3.12 clearly show the building up of a starting vortex in the simulation as reported by Voropayev *et al.* (1999) in experiments. We should note that the vorticity shown in these images will decay with time but scalar tracers like dyes will not decay as fast since molecular diffusion is three orders of magnitude slower than momentum diffusion. Hence, in experiments the large dipole structures will have a very high contrast when compared with the equivalent vorticity plots.

In Fig. 3.13 the variation of the velocity and net force (thrust - drag) generated by the self-propelling body with time are shown. The plots shows that the body is

accelerating as the net force slowly drops. In Fig. 3.14, the velocity profile across the wake of two bodies, one accelerating and the other decelerating, is shown. The velocity profile shows the central positive velocity zone corresponding to the thrust generated by the thrusters and the outer negative velocity zone which corresponding to the body drag. The relative areas under the two zones determines whether the wake has positive or negative momentum. The difference between the wakes of an accelerating and decelerating body is clearly seen with the accelerating wake showing larger area under positive velocity and the decelerating wake with more negative velocity.

3.5 Discussion

We have shown the capability of the discrete vortex methods in different test cases and also applied it to a novel self-propelled model. The preliminary results we have obtained are promising and the code can be used for full-scale simulation of similar flows. This approach is also ideally suited to perform studies of fish locomotion.

(a) Vortex blobs

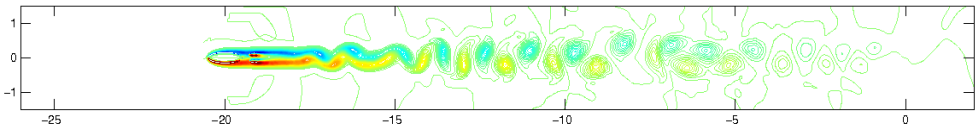

(b) Vorticity contour

Figure 3.8: Corresponding vortex kernel locations and the vorticity contour for a towed model

(a) t = 0

(b) t = 5

(c) t = 10

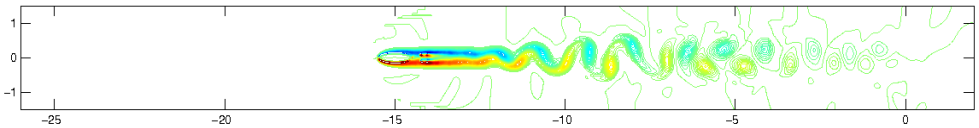

(d) t = 15

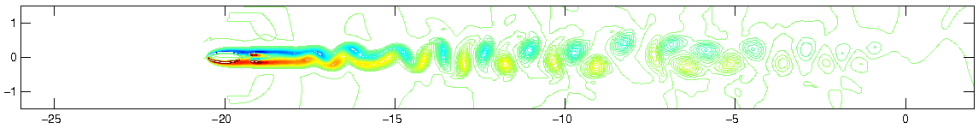

(e) t = 20

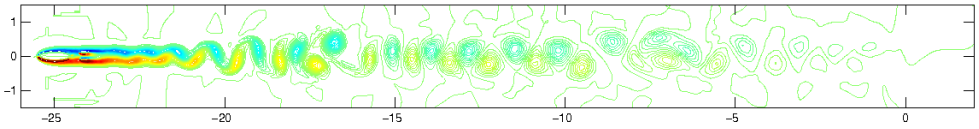

(f) t = 25

Figure 3.9: Vorticity contours of the model being towed at a uniform velocity at $Re = 1000$

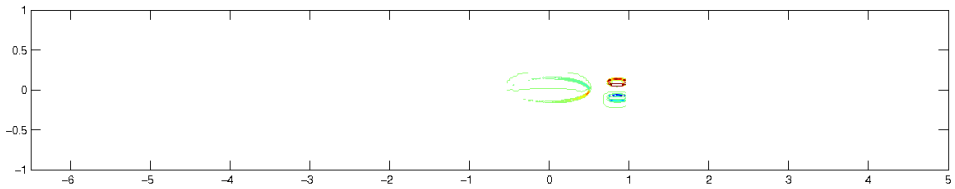

(a) t = 0

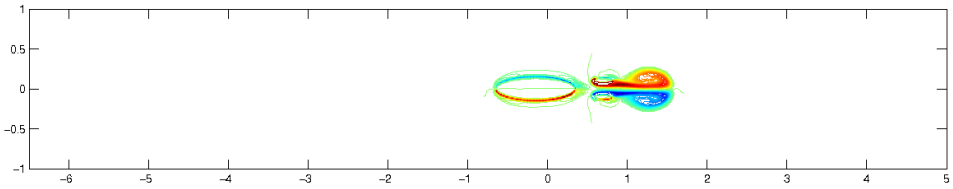

(b) t = 0.5

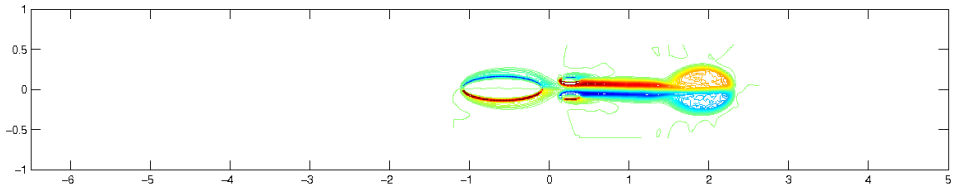

(c) t = 1.0

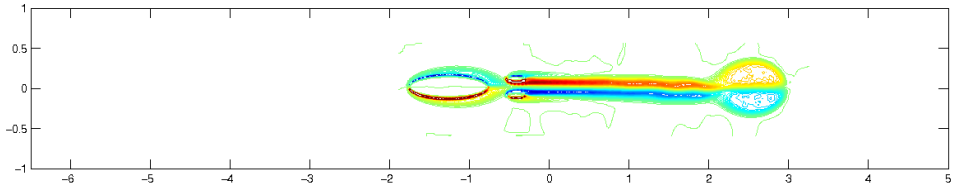

(d) t = 1.5

Figure 3.10: Vorticity contours of self-propelled model accelerating from zero velocity at $Re = 1000$

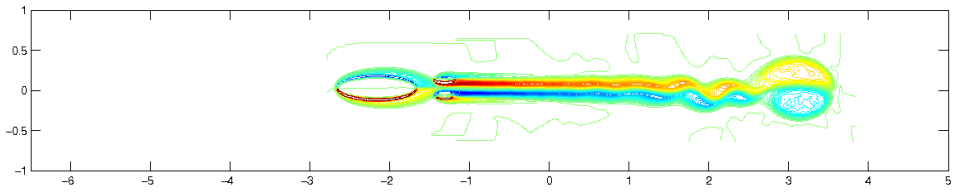

(a) t = 2.0

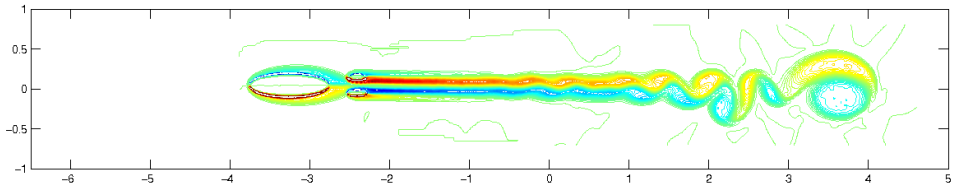

(b) t = 2.5

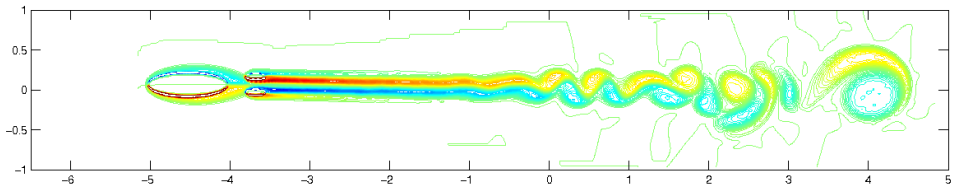

(c) t = 3.0

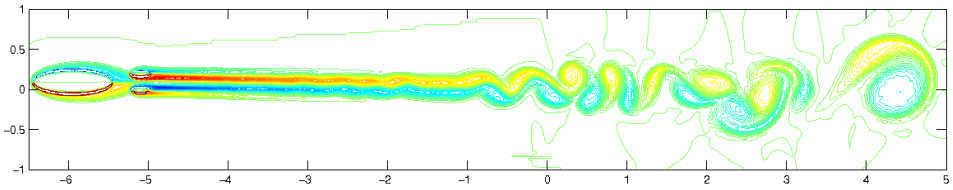

(d) t = 3.5

Figure 3.11: Vorticity contours of self-propelled model accelerating from zero velocity at $Re = 1000$

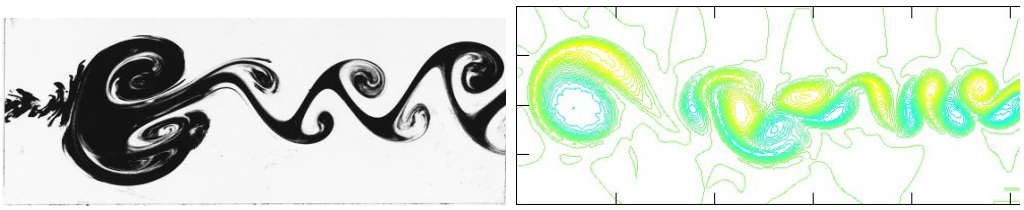

(a) Experiments performed by Voropayev *et al.* (1999)

(b) Simulation

Figure 3.12: Comparison of dipole structures formed by the acceleration phase of a self-propelled body

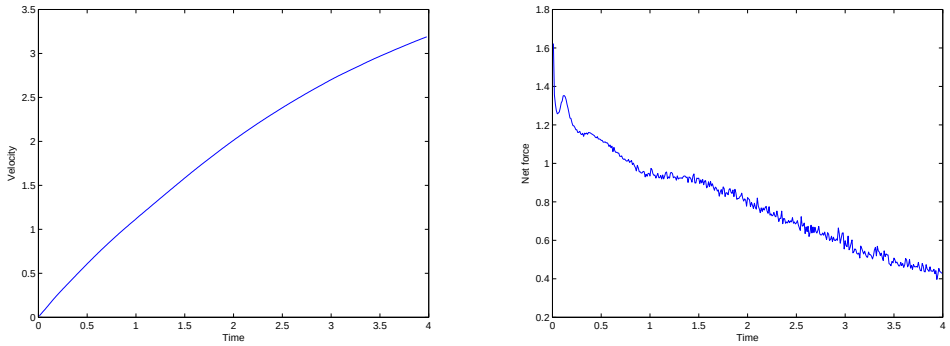

(a) Velocity vs time

(b) Net force vs time

Figure 3.13: Velocity and net force of the self-propelled model accelerating from zero velocity at $Re = 1000$

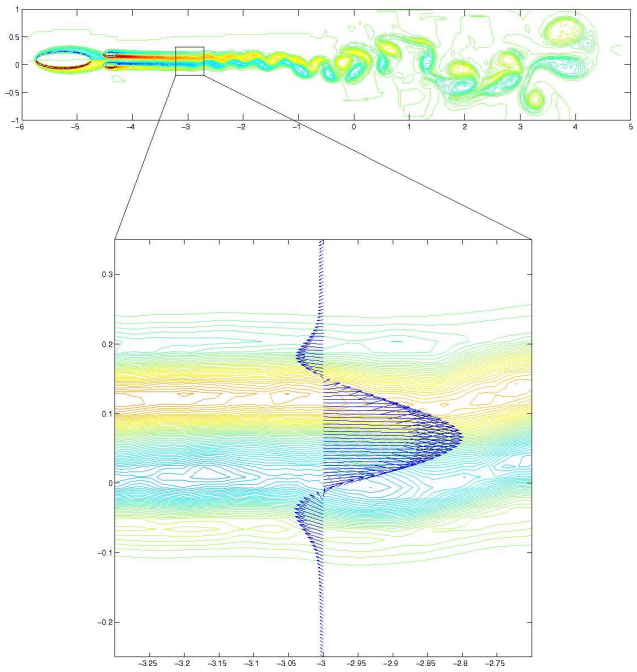

(a) Wake of accelerating body

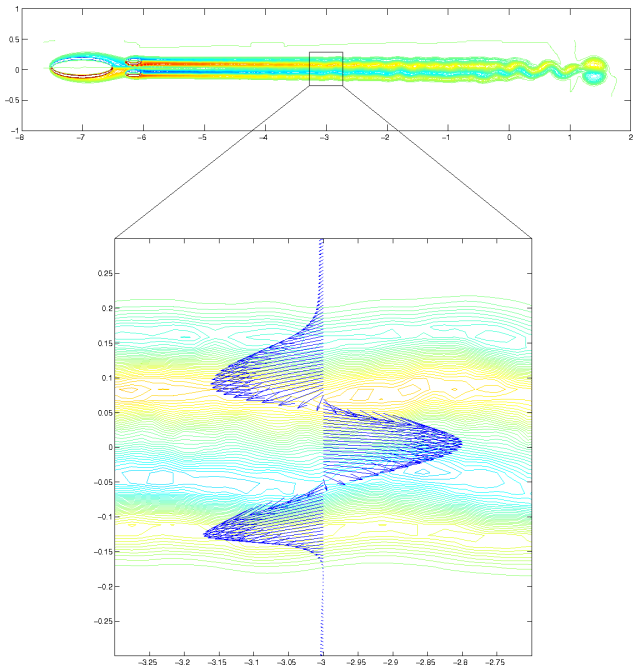

(b) Wake of decelerating body

Figure 3.14: Velocity along the cross-section of two wakes

CHAPTER 4

CONCLUSION

An experimental facility was built to study jets and wakes in a stratified medium with the provision to do PLIF, dye and Synthetic Schlieren flow visualization. In this apparatus we can achieve tow speeds upto $5cm/s$. For a model with a diameter of $3.5cm$, this tow speed capability corresponds to a maximum Reynolds number of 1750.

We have shown the difference between wakes in a stratified and unstratified fluid environment. The observations conform to those reported in literature. The homogeneous fluid results in an axisymmetric wake expanding equally in all directions. The wake in a stratified fluid with an $Fr \in [1, 2]$ and $Re \in [600, 700]$ results in an asymmetric vortex shedding. A turbulent propelled jet with a $Re \in [23,800, 47,600]$ and $Fr \in [65, 130]$ expands vertically to a maximum height and then collapses to a height a few rotor diameters. We also clearly see the internal gravity waves produced by the collapsing turbulent jet in the synthetic Schlieren images. Horizontally, the jet keeps expanding until it reaches the side walls of the tank. A feature that was observed and may be of importance is the backflow observed in the vertical plane at the periphery of the jet. As the turbulent flow expands and collapses, the flow just above and below the jet are advected in the opposite direction. This may explain the observation documented by Sheres & Munk (1992). The submarine could have induced a similar reverse flow at the surface as seen by the hose deformation.

The effect of the jets on the fluid surface indicates that stratification prevents most of the direct effects of the turbulent jet from being detected. As the jet itself does not rise to the surface any surface deformation can only be caused by the pressure field generated by the body. A Bernoulli hump and the Kelvin wave can certainly be observed but the amplitude of the hump decays with the depth and below a certain depth they would be undetectable. The internal gravity waves from the collapsing jet will certainly reach the surface but whether they will cause a significant signature which can be seen by either SAR images or sea surface height data from remote observations is not known.

A novel self-propelled two-dimensional model has been demonstrated to work. Although there is a temptation to compare two-dimensional flow data with the quasi two-dimensional collapsed wakes in a stratified flow, we should resist the temptation simply because the damping from the adjacent layer to a collapsed wake is significant and hence cannot be two-dimensional. The model is however a stepping stone is observing a self-propelled body in motion and can easily be extended to simulate a swimming fish owing to the easy adaptability of vortex methods to complicated boundary surfaces. We have achieved our goal of developing a numerical tool which can help us better understand the decay of late wakes in two-dimensional environment.

References

Afanasyev, Y. D. 2004 Wakes behind towed and self-propelled bodies: Asymptotic theory. *Physics of Fluids* **16** (8), 3235–3238.

Afanasyev, Y. D. & Korabel, V. N. 2004 Starting vortex dipoles in a viscous fluid: asymptotic theory, numerical simulations, and laboratory experiments. *Physics of Fluids* **16** (11), 3850–3858.

Billant, P. & Chomaz, J.-M. 2001 Self-similarity of strongly stratified inviscid flows. *Physics of Fluids* **13** (6), 1645–1651.

Bonneton, P., Chomaz, J. M. & Hopfinger, E. J. 1993 Internal waves produced by the turbulent wake of a sphere moving horizontally in a stratified fluid. *J. Fluid Mech.* **254**, 23–40.

Brandt, L. K. & Nomura, K. K. 2006 The physics of vortex merger: Further insight. *Physics of Fluids* **18**, 051701.1–051701.4.

Chomaz, J. M., Bonneton, P., Butet, A. & Hopfinger, E. J. 1993*a* Vertical diffusion of the far wake of a sphere in a stratified fluid. *Phys. Fluids A* **5** (11), 2799–2806.

Chomaz, J. M., Bonneton, P. & Hopfinger, E. J. 1993*b* The structure of the near wake of a sphere moving horizontally in a stratified fluid. *J. Fluid Mech.* **254**, 1–21.

Chorin, A. J. 1973 Numerical study of slightly viscous flow. *J. Fluid Mech.* **57**, 785–796.

Clarke, N. R. & Tutty, O. R. 1994 Construction and validation of a discrete vortex method for the two-dimensional incompressible navier-stokes equations. *Computers and Fluids* **23** (6), 751–793.

Cottet, G.-H., Koumoutsakos, P. & Salihi, M. L. O. 2000 Vortex methods with spatially varying cores. *Journal of Compuational Physics* **162**, 164–185.

van Dommelen, L. & Rundensteiner, E. A. 1989 Fast, adaptive summation of point forces in the two-dimensional poisson equation. *Journal of Computational Physics* **83**, 126–147.

Draghicescu, C. I. & Draghicescu, M. 1995 A fast algorithm for vortex blob interactions. *Journal of Compuatational Physics* **116**, 69–78.

Fritts, D., Gourlay, M., Orlando, W., Meyer, C., Werne, J. & Lund, T. 2003 Numerical simulation of late wakes in stratified and sheared flows. *Proceedings of the 2003 User Group Conference* pp. 206–210.

Greengard, C. 1985 The core spreading vortex method approximates the wrong equation. *Journal of Computational Physics* **61**, 345–348.

Greengard, L. & Rokhlin, V. 1997 A fast algorithm for particle simulations. *Journal of Computational Physics* **135**, 280–292.

Hill, D. F. 2002 General density gradients in general domains: the "two-tank" method revisited. *Experiments in Fluids* **32**, 434–440.

Leonard, A. 1980 Vortex methods for flow simulation. *Journal of Computational Physics* **37**, 289–335.

Lin, J. T. & Pao, Y. H. 1979 Wakes in stratified fluids. *Ann. Rev. Fluid Mech.* **11**, 317–338.

Lin, Q., Lindberg, W. R., Boyer, D. L. & Fernando, H. J. S. 1992 Stratified flow past a sphere. *J. Fluid Mech.* **240**, 315–354.

Mas-Gallic, S. & Raviart, P. A. 1987 Particle approximation of convection diffusion problems. *Tech. Rep.*. Laboratoire dAnalyse Numerique d IUniversite Pierre et Marie Curie.

Melsheimer, C. 2001 *Ship wakes observed with ERS and SPOT*. Centre for Remote Imaging, Sensing and Processing.

Meunier, P. 2006 Self-preservation in stratified momentum wakes. *Physics of Fluids* **18** (10), 106601.1–106601.10.

Meunier, P. & Spedding, G. R. 2004 A loss of memory in stratified momentum wakes. *Physics of Fluids* **16** (2), 298–305.

Meunier, P. & Spedding, G. R. 2006 Stratified propelled wakes. *J. Fluid Mech.* **552**, 229–256.

Ogami, Y. & Akamatsu, T. 1991 Viscous flow simulation using the discrete vortex model-the diffusion velocity model. *Comput. Fluids* **19**, 433–441.

Qian, L. & Vezza, M. 2001 A vorticity-based method for incompressible unsteady viscous flows. *Journal of Computational Physics* **172**, 515–542.

Reed, A. M. & Milgram, J. H. 2002 Ship wakes and their radar images. *Annu. Rev. Fluid Mech.* **34**, 469–502.

Rossi, L. F. 1996 Resurrecting core spreading vortex methods: A new scheme that is both deterministic and convergent. *SIAM J. Sci. Comput.* **17**, 370397.

Saffman, P. G. 1992 *Vortex dynamics*. Cambridge University Press.

Sarkar, S. 2004 Incompressible viscous flow past an oscillating airfoil. PhD thesis, Indian Institute of Science.

Schooley, A. H. & Stewart, R. W. 1963 Experiments with a self-propelled body submerged in a fluid with a vertical density gradient. *J. Fluid Mech.* **15**, 83–96.

Sheres, D. & Munk, W. 1992 On john isaacs' 1952 measurements of surface-ship and submarine wakes. *Oceanography* **5** (2), 121–123.

Subramaniam, S. 1996 A new mesh-free vortex method. PhD thesis, Florida State University.

Voropayev, S. I., Fernando, H. J. S., Smirnov, S. A. & Morrison, R. 2007 On surface signatures generated by submerged momentum sources. *Physics of Fluids* **19**, 076603.1–076603.10.

Voropayev, S. I., McEachern, G. B., Fernando, H. J. S. & Boyer, D. L. 1999 Large vortex structures behind a maneuvering body in stratified fluids. *Physics of Fluids* **11** (6), 1682–1684.

Voropayev, S. I. & Smirnov, S. A. 2003 Vortex streets generated by a moving momentum source in a stratified fluid. *Physics of Fluids* **15** (3), 618–624.

Williamson, C. H. K. 1988 Defining a universal and continuous strouhal-reynolds number relationship for the laminar vortex shedding of a circular cylinder. *Phys. Fluids* **31** (10), 2742–2744.

Wren, G. G. & May, D. 1997 Detection of submerged vessels using remote sensing techniques. *Australian Defence Force Journal* **127**, 9–15.